Kalman Filtering for Relative Inertial Navigation of Uninhabited Air Vehicles

Adam M. Fosbury* and John L. Crassidis†

University at Buffalo, State University of New York, Amherst, NY, 14260-4400

An extended Kalman filter is derived for estimating the relative position and attitude of a pair of uninhabited air vehicles, designated leader and follower. All leader states are assumed known, while the relative states are estimated using line-of-sight measurements between the vehicles along with angular rate and acceleration measurements of the follower. Noise is present on all measurements, while biases are present only on the latter two. Line-of-sight measurements are generated using visual navigation beacons. The global attitude is parameterized using a quaternion, while the local attitude error is given by a three-dimensional attitude representation. The quaternion normalization constraint is maintained using a multiplicative error quaternion. Simulation results show that the relative states and measurement biases converge within their respective covariance bounds. The number of visual navigation beacons is shown to affect estimator convergence in the presence of initial condition errors.

I. Introduction

Formation flight of aircraft has been an active and growing area of study in recent years. Maintaining a desired spatial formation requires accurate knowledge of the relative position and speed between the individual vehicles. Control algorithms designed for formation flight are given in Ref. 1–5. Johnson et al.[6] demonstrate a vision-based method of formation control and state estimation. Two approaches are used. The first incorporates an extended Kalman filter (EKF) developed in Ref. 7 with camera based images to determine the relative states. The second approach uses image size and location to directly regulate the control algorithm.

The integration of Global Positioning System (GPS) signals with Inertial Measurement Units (IMUs) has become a standard approach for position and attitude determination of a moving vehicle. An Inertial Navigation System (INS) is best described in the Preface section of the excellent book by Chatfield,[8] who states "Inertial navigation involves a blend of inertial measurements, mathematics, control system design, and geodesy." Historically, INS's were primarily used for military and commercial aircraft applications due to their high cost. However, with the advent of cheaper sensors, especially micro-mechanical ones,[9] several new applications have become mainstream, including uninhabited air vehicles, micro-robots, and even guided munitions.[‡] Although these cheaper sensors do not perform as well as high-grade sensors in terms of drift and white-noise measurement errors, they can be used to meet the requirements of several vehicle position/attitude knowledge specifications when aided with GPS. This allows for an attractive approach since a completely self-contained system can be used to calibrate IMUs online using GPS-determined position observations, while also determining vehicle attitude and rates in realtime. By far the primary mechanism historically used to blend GPS measurements with IMU data has been the extended Kalman filter (EKF).[10] Other implementations include an unscented Kalman filter[11] and particle filters.[12]

The earliest discussion on the use of GPS and an INS for relative navigation occurs in Ref. 13. Relative position is propagated using a linear discrete equation, though the exact form of the state transition matrix

*Graduate Student, Department of Mechanical & Aerospace Engineering, Email: fosbury@eng.buffalo.edu. Student Member AIAA

†Associate Professor, Department of Mechanical & Aerospace Engineering, Email: johnc@eng.buffalo.edu. Associate Fellow AIAA.

‡See http://www.airpower.maxwell.af.mil/airchronicles/cc/pinker.html for recent contributions of GPS/INS to Air Force competencies.

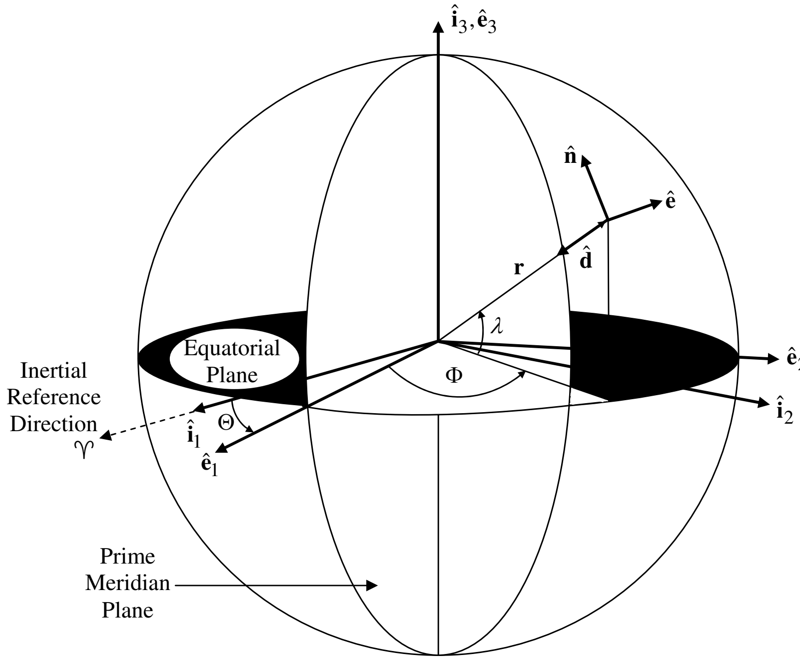

Figure 1. Definitions of Various Reference Frames

is not provided. Increased accuracy is achieved due to the high correlation of GPS errors aboard the leader and follower. The results are extended to vehicle platooning in Ref. 14.

This paper examines the use of INS equations for relative navigation of a formation of uninhabited air vehicles (UAVs). INS equations are developed for a two-UAV system. An extended Kalman filter is derived for estimation of the relative position and relative attitude between the two aircraft. Relative attitude is parameterized using the four-component quaternion. Measurements between the UAVs are made using the vision-based navigation (VISNAV) system discussed in Ref. 15. This consists of an optical sensor combined with a specific light source (beacon) in order to achieve a selective vision. The sensor is made up of a Position Sensing Diode (PSD) placed in the focal plane of a wide angle lens, yielding a one hundred degree field of view. When the rectangular silicon area of the PSD is illuminate by energy from a beacon focused by the lens, it generates electrical currents in four directions the can be processed to estimate the energy centroid of the image. This is then used to determine the line-of-sight (LOS) vector between the sensor and the beacon.

The VISNAV system is applied to the spacecraft formation flying problem in Ref. 16. State estimation is performed using an optimal observer design. Simulations show that accurate estimates of relative position and attitude are possible. A predictive filter is combined with the VISNAV system for estimation of relative position and attitude in Ref. 17. Kim et al. apply an extended Kalman filter to the VISNAV-based relative position and attitude estimation problem in Ref. 18. The effects of beacon location errors on estimation accuracy are analyzed in Ref. 19. In this current work, the aforementioned previous work is expanded for relative navigation between UAVs using LOS observations.

The organization of this paper is as follows. First, a summary of the various coordinate frames used in the theoretical developments is provided. This is followed by a review of quaternion attitude parameters and the associated kinematics. The relative INS equations are then derived. Next, an EKF for estimation of relative position and attitude is developed. Finally, simulations are performed to demonstrate the effectiveness of the filter.

II. Reference Frames

This section summarizes the various reference frames used in the remainder of this paper, as shown in Figure 1:

- Earth-Centered-Inertial (ECI): denoted by $\{\hat{\mathbf{i}}_1, \hat{\mathbf{i}}_2, \hat{\mathbf{i}}_3\}$. The origin is at the center of the Earth, with the $\hat{\mathbf{i}}_1$ axis pointing in the direction of the vernal equinox, the $\hat{\mathbf{i}}_3$ axis pointing towards the North pole, while $\hat{\mathbf{i}}_2$ completes the right-handed coordinate system. This frame is fixed in space, with associated vectors identified by the letter I.

- Earth-Centered-Earth-Fixed (ECEF): denoted by $\{\hat{\mathbf{e}}_1, \hat{\mathbf{e}}_2, \hat{\mathbf{e}}_3\}$. The origin of this frame is also located at the center of the Earth. The primary difference is that this frame rotates with the Earth. The $\hat{\mathbf{e}}_3\}$ axis points towards the north pole and is equal to $\hat{\mathbf{i}}_3$. The $\hat{\mathbf{e}}_1$ axis is directed toward the prime meridian, and the $\hat{\mathbf{e}}_2$ axis completes the right-handed system. The letter E signifies a vector defined with respect to this reference frame.

- North-East-Down (NED): denoted by $\{\hat{\mathbf{n}}, \hat{\mathbf{e}}, \hat{\mathbf{d}}\}$. This reference frame is formed by fitting a tangent plane to the geodetic reference ellipse at a given point of interest.[10] The $\hat{\mathbf{n}}$ axis points North, the $\hat{\mathbf{e}}$ axis is directed East, and the $\hat{\mathbf{d}}$ axis completes the right-handed system. This reference frame is generally used for local navigation purposes. The letter N signifies a vector defined with respect to this reference frame.

- Body Frames: denoted by $\{\hat{\mathbf{b}}_1, \hat{\mathbf{b}}_2, \hat{\mathbf{b}}_3\}$. These are fixed to the vehicle body, rotating with it. Body frames fixed to the two UAVs are designated leader (l) and follower (f).

The convention applied in this paper is to use these letters as a superscript following the vector or matrix that is being described.

Transformations between reference frames are made using direction cosine or attitude matrices. A transform from the inertial frame to a generic body frame B is mathematically described as

$$\left\{ \begin{array}{c} \hat{\mathbf{b}}_1 \\ \hat{\mathbf{b}}_2 \\ \hat{\mathbf{b}}_3 \end{array} \right\} = \left[\begin{array}{ccc} \cos\alpha_{11} & \cos\alpha_{12} & \cos\alpha_{13} \\ \cos\alpha_{21} & \cos\alpha_{22} & \cos\alpha_{23} \\ \cos\alpha_{31} & \cos\alpha_{32} & \cos\alpha_{33} \end{array} \right] \left\{ \begin{array}{c} \hat{\mathbf{i}}_1 \\ \hat{\mathbf{i}}_2 \\ \hat{\mathbf{i}}_3 \end{array} \right\} = A_I^B \left\{ \begin{array}{c} \hat{\mathbf{i}}_1 \\ \hat{\mathbf{i}}_2 \\ \hat{\mathbf{i}}_3 \end{array} \right\} \tag{1}$$

where α_{ij} is the angle between the i^{th} body unit vector and the j^{th} inertial unit vector. A_I^B is the attitude matrix.

An overview of the conversion between the ECEF and NED reference frames is provided here. For a more complete discussion, see Ref. 10. Given the latitude (λ), longitude (ϕ), and height (h), the ECEF coordinates are given by the equations

$$x = (N + h)\cos\lambda\cos\phi \tag{2a}$$

$$y = (N + h)\cos\lambda\sin\phi \tag{2b}$$

$$z = [N(1 - e^2) + h]\sin\lambda \tag{2c}$$

where $e = 0.0818$ is the eccentricity of the Earth's ellipsoid, and N is the length of the normal to the ellipsoid given by the equation

$$N = \frac{a}{\sqrt{1 - e^2 \sin^2\lambda}} \tag{3}$$

a is the semimajor axis of the ellipsoid and is equal to 6,378,137 meters. The direction cosine matrix relating the two reference frames is given in Ref. 10:

$$A_E^N = \left[\begin{array}{ccc} -\sin\lambda\cos\phi & -\sin\lambda\sin\phi & \cos\lambda \\ -\sin\phi & \cos\phi & 0 \\ -\cos\lambda\cos\phi & -\cos\lambda\sin\phi & -\sin\lambda \end{array} \right] \tag{4}$$

The concept of Euler angles are often used to provide a more physical interpretation of attitude parameters. These parameters define the attitude as three successive rotations about sequentially displaced body axes. The Euler rotation about the i^{th} body axis, $M_i(\theta)$, is given by

$$M_1(\theta) = \begin{bmatrix} 1 & 0 & 0 \\ 0 & \cos\theta & \sin\theta \\ 0 & -\sin\theta & \cos\theta \end{bmatrix} \tag{5a}$$

$$M_2(\theta) = \begin{bmatrix} \cos\theta & 0 & -\sin\theta \\ 0 & 1 & 0 \\ \sin\theta & 0 & \cos\theta \end{bmatrix} \tag{5b}$$

$$M_3(\theta) = \begin{bmatrix} \cos\theta & \sin\theta & 0 \\ -\sin\theta & \cos\theta & 0 \\ 0 & 0 & 1 \end{bmatrix} \tag{5c}$$

For an (α, β, γ) Euler sequence with angles $\theta_1, \theta_2, \theta_3$, the direction cosine matrix (DCM) will be given by

$$A = M_\gamma(\theta_3) M_\beta(\theta_2) M_\alpha(\theta_1) \tag{6}$$

In the simulations shown later in this paper, the errors will be computed based on a (3,2,1) sequence using roll (ψ), pitch (θ) and yaw (ϕ) angles. The corresponding DCM is

$$\begin{aligned} A &= \begin{bmatrix} 1 & 0 & 0 \\ 0 & \cos\phi & \sin\phi \\ 0 & -\sin\phi & \cos\phi \end{bmatrix} \begin{bmatrix} \cos\theta & 0 & -\sin\theta \\ 0 & 1 & 0 \\ \sin\theta & 0 & \cos\theta \end{bmatrix} \begin{bmatrix} \cos\psi & \sin\psi & 0 \\ -\sin\psi & \cos\psi & 0 \\ 0 & 0 & 1 \end{bmatrix} \\ &= \begin{bmatrix} c\theta c\psi & c\theta s\psi & -s\theta \\ s\phi s\theta c\psi - c\phi s\psi & s\phi s\theta s\psi + c\phi c\psi & s\phi c\theta \\ c\phi s\theta c\psi + s\phi s\psi & c\phi s\theta s\psi - s\phi c\psi & c\phi c\theta \end{bmatrix} \end{aligned} \tag{7}$$

where $c\theta = \cos\theta$, and $s\theta = \sin\theta$. When the DCM is known, the corresponding Euler angles can be computed from the individual elements by the following equations:[20]

$$\psi = \tan^{-1}\left(\frac{A_{12}}{A_{11}}\right) \tag{8a}$$

$$\theta = -\sin^{-1}(A_{13}) \tag{8b}$$

$$\phi = \tan^{-1}\left(\frac{A_{23}}{A_{33}}\right) \tag{8c}$$

III. Attitude Kinematics

A variety of parameterizations can be used to specify attitude including Euler angles, quaternions, and Rodrigues parameters.[21] This paper uses the quaternion, which is based off of the Euler angle/axis parameterization. The quaternion is defined as $\mathbf{q} \equiv [\ \mathbf{q}_{13}^T \quad q_4\ ]^T$ with $\mathbf{q}_{13} = [\ q_1 \quad q_2 \quad q_3\ ]^T = \hat{\mathbf{e}} \sin(\nu/2)$, and $q_4 = \cos(\nu/2)$, where $\hat{\mathbf{e}}$ and ν are the Euler axis of rotation and rotation angle, respectively. This vector must satisfy the constraint $\mathbf{q}^T\mathbf{q} = 1$. The attitude matrix can be written as a function of the quaternion:

$$A = \Xi^T(\mathbf{q})\Psi(\mathbf{q}) \tag{9}$$

where

$$\Xi(\mathbf{q}) \equiv \begin{bmatrix} q_4 I_{3\times3} + [\mathbf{q}_{13}\times] \\ -\mathbf{q}_{13}^T \end{bmatrix} \tag{10a}$$

$$\Psi(\mathbf{q}) \equiv \begin{bmatrix} q_4 I_{3\times3} - [\mathbf{q}_{13}\times] \\ -\mathbf{q}_{13}^T \end{bmatrix} \tag{10b}$$

with

$$[\mathbf{q}_{13}\times] = \begin{bmatrix} 0 & -q_3 & q_2 \\ q_3 & 0 & -q_1 \\ -q_2 & q_1 & 0 \end{bmatrix} \tag{11}$$

The attitude kinematic equation is given by[20]

$$\dot{A}_I^B = -[\boldsymbol{\omega}_{B|I}^B\times]A_I^B \tag{12}$$

where $\boldsymbol{\omega}_{B|I}^B$ is the angular velocity of the body frame with respect to the inertial frame, given in body frame coordinates, and A_I^B is the attitude matrix that converts from the body frame to the inertial frame.

The relative quaternion $\mathbf{q}_{f|l}$ and corresponding attitude matrix are defined by

$$\mathbf{q}_{fl} \equiv \mathbf{q}_f \otimes \mathbf{q}_l^{-1} \tag{13a}$$

$$A_l^f \equiv A(\mathbf{q}_{f|l}) = A(\mathbf{q}_f)A^T(\mathbf{q}_l) \tag{13b}$$

which are consistent with Refs. 21 and 22. The symbol $\otimes$ denotes the quaternion multiplication, given by

$$\mathbf{q}_a \otimes \mathbf{q}_b \equiv \begin{bmatrix} \Psi(\mathbf{q}_a) & \mathbf{q}_a \end{bmatrix} \mathbf{q}_b = \begin{bmatrix} \Xi(\mathbf{q}_b) & \mathbf{q}_b \end{bmatrix} \mathbf{q}_a \tag{14}$$

and $\mathbf{q}^{-1}$ is the quaternion inverse, defined by

$$\mathbf{q}^{-1} \equiv \begin{bmatrix} -q_1 & -q_2 & -q_3 & q_4 \end{bmatrix}^T \tag{15}$$

Reference 23 shows the quaternion kinematics to be given by

$$\dot{\mathbf{q}}_{f|l} = \frac{1}{2}\Xi(\mathbf{q}_{f|l})\boldsymbol{\omega}_{f|l}^f \tag{16}$$

where $\boldsymbol{\omega}_{f|l}^f$ is the relative angular velocity defined as

$$\boldsymbol{\omega}_{f|l}^f \equiv \boldsymbol{\omega}_{f|E}^f - A_l^f \boldsymbol{\omega}_{l|E}^l \tag{17}$$

To reduce the computational load, a discrete form of the quaternion propagation is used. This is given in Ref. 23 as

$$\mathbf{q}_{fl_{k+1}} = \bar{\Omega}(\boldsymbol{\omega}_{f_k}^f)\bar{\Gamma}(\boldsymbol{\omega}_{l_k}^l)\mathbf{q}_{fl_k} \tag{18}$$

where

$$\bar{\Omega}(\boldsymbol{\omega}_{f_k}^f) \equiv \begin{bmatrix} \cos\left(\frac{1}{2}\|\boldsymbol{\omega}_{f_k}^f\|\Delta t\right) I_{3\times 3} - [\boldsymbol{\psi}_k\times] & \boldsymbol{\psi}_k \\ -\boldsymbol{\psi}_k^T & \cos\left(\frac{1}{2}\|\boldsymbol{\omega}_{f_k}^f\|\Delta t\right) \end{bmatrix} \tag{19a}$$

$$\boldsymbol{\psi}_k \equiv \frac{\sin\left(\frac{1}{2}\|\boldsymbol{\omega}_{f_k}^f\|\Delta t\right)\boldsymbol{\omega}_{f_k}^f}{\|\boldsymbol{\omega}_{f_k}^f\|} \tag{19b}$$

$$\bar{\Gamma}(\boldsymbol{\omega}_{l_k}^l) \equiv \begin{bmatrix} \cos\left(\frac{1}{2}\|\boldsymbol{\omega}_{l_k}^l\|\Delta t\right) I_{3\times 3} - [\boldsymbol{\zeta}_k\times] & -\boldsymbol{\zeta}_k \\ \boldsymbol{\zeta}_k^T & \cos\left(\frac{1}{2}\|\boldsymbol{\omega}_{l_k}^l\|\Delta t\right) \end{bmatrix} \tag{19c}$$

$$\boldsymbol{\zeta}_k \equiv \frac{\sin\left(\frac{1}{2}\|\boldsymbol{\omega}_{l_k}\|\Delta t\right)\boldsymbol{\omega}_{l_k}}{\|\boldsymbol{\omega}_{l_k}\|} \tag{19d}$$

and Δt is the sampling interval.

IV. Relative INS Equations

The relative INS equations to be used in the extended Kalman filter are developed in this section. The relative position vector is defined as

$$\begin{aligned} \mathbf{r}_{f|l}^{f} &= \mathbf{r}_{f|I}^{f} - A_l^f \mathbf{r}_{l|I}^{l} \\ &= A_l^f A_E^l A_I^E (\mathbf{r}_{f|I}^{I} - \mathbf{r}_{l|I}^{I}) \end{aligned} \tag{20}$$

where A_I^E is the attitude matrix which converts from the inertial frame to the ECEF frame. The corresponding angular velocity is $\boldsymbol{\omega}_{E|I}^E = [\begin{array}{ccc} 0 & 0 & \omega_e \end{array}]^T$, where ω_e is the Earth's rotational rate.

Taking two time derivatives of Eq. (20) gives

$$\begin{aligned} \ddot{\mathbf{r}}_{f|l}^{f} &= \frac{d^2}{dt^2}\left(\mathbf{r}_{f|l}^{f}\right) \\ &= \frac{d^2}{dt^2}\left(A_l^f A_E^l A_I^E\right)(\mathbf{r}_{f|I}^{I} - \mathbf{r}_{l|I}^{I}) + 2\frac{d}{dt}\left(A_l^f A_E^l A_I^E\right)\frac{d}{dt}(\mathbf{r}_{f|I}^{I} - \mathbf{r}_{l|I}^{I}) + A_l^f A_E^l A_I^E \frac{d^2}{dt^2}\left(\mathbf{r}_{f|I}^{I} - \mathbf{r}_{l|I}^{I}\right) \end{aligned} \tag{21}$$

and using the appropriate identities and substitutions yields

$$\begin{aligned} \ddot{\mathbf{r}}_{f|l}^{f} &= -[(\dot{\boldsymbol{\omega}}_{f|E}^{f})\times]\mathbf{r}_{f|l}^{f} - [(\boldsymbol{\omega}_{f|I}^{f})\times][(\boldsymbol{\omega}_{f|I}^{f})\times]\mathbf{r}_{f|l}^{f} + [(\boldsymbol{\omega}_{f|I}^{f} \times A_l^f A_E^l \boldsymbol{\omega}_{E|I}^{E})\times]\mathbf{r}_{f|l}^{f} - 2[(\boldsymbol{\omega}_{f|I}^{f})\times]\dot{\mathbf{r}}_{f|l}^{f} \\ &\quad + \ddot{\mathbf{r}}_{f|I}^{I} - \ddot{\mathbf{r}}_{l|I}^{I} \end{aligned} \tag{22}$$

The inertial accelerations of the leader and follower are given by Newton's law:

$$\ddot{\mathbf{r}}_{l|I}^{I} = \mathbf{a}_l^I + \mathbf{g}_l^I \tag{23a}$$

$$\ddot{\mathbf{r}}_{f|I}^{I} = \mathbf{a}_f^I + \mathbf{g}_f^I \tag{23b}$$

The gravity model in ECEF coordinates is given by

$$\mathbf{g}^E = \frac{-\mu}{\|\mathbf{r}^E\|^3}\mathbf{r}^E \tag{24}$$

where $\mu = 3.986 \times 10^5$ km^3/s^2. Equation (24) provides the only nonlinear term relative acceleration equation. Equation (22) is then written as

$$\begin{aligned} \ddot{\mathbf{r}}_{f|l}^{f} &= -[(\dot{\boldsymbol{\omega}}_{f|E}^{f})\times]\mathbf{r}_{f|l}^{f} - [(\boldsymbol{\omega}_{f|I}^{f})\times][(\boldsymbol{\omega}_{f|I}^{f})\times]\mathbf{r}_{f|l}^{f} + [(\boldsymbol{\omega}_{f|I}^{f} \times A_l^f A_E^l \boldsymbol{\omega}_{E|I}^{E})\times]\mathbf{r}_{f|l}^{f} - 2[(\boldsymbol{\omega}_{f|I}^{f})\times]\dot{\mathbf{r}}_{f|l}^{f} \\ &\quad + \mathbf{a}_f^f - A_l^f \mathbf{a}_l^l + A_l^f A_E^l \left(\mathbf{g}_f^E - \mathbf{g}_l^E\right) \end{aligned} \tag{25}$$

The acceleration measurement model is defined as

$$\tilde{\mathbf{a}}_f^f = \mathbf{a}_f^f + \mathbf{b}_{fa} + \boldsymbol{\eta}_{fav} \tag{26a}$$

$$\dot{\mathbf{b}}_{fa} = \boldsymbol{\eta}_{fau} \tag{26b}$$

where $\mathbf{b}_{fa}$ is the accelerometer bias and $\boldsymbol{\eta}_{fav}$ and $\boldsymbol{\eta}_{fau}$ are zero-mean Gaussian white noise processes. Their respective spectral densities are $\sigma_{av}^2 I_{3\times3}$ and $\sigma_{au}^2 I_{3\times3}$.

The gyro measurement model has a similar form:

$$\tilde{\boldsymbol{\omega}}_{f|I}^{f} = \boldsymbol{\omega}_{f|I}^{f} + \mathbf{b}_{fg} + \boldsymbol{\eta}_{fgv} \tag{27a}$$

$$\dot{\mathbf{b}}_{fg} = \boldsymbol{\eta}_{fgu} \tag{27b}$$

where $\boldsymbol{\eta}_{fgv}$ and $\boldsymbol{\eta}_{fgu}$ are zero-mean Gaussian white noise processes with spectral densities $\sigma_{gv}^2 I_{3\times3}$ and $\sigma_{gu}^2 I_{3\times3}$. $\mathbf{b}_{fg}$ is the gyro bias. See the appendix of Ref. 11 for a more detailed discussion on the gyro bias model.

V. Extended Kalman Filter Equations

This section shows the development of an extended Kalman filter for estimation of relative position and attitude. The states of interest are relative attitude, relative position, relative velocity, and biases on the inertial acceleration and angular velocity measurements:

$$\mathbf{x} = \begin{bmatrix} \mathbf{q}_{f|l}^T & (\mathbf{r}_{f|l}^f)^T & (\dot{\mathbf{r}}_{f|l}^f)^T & \mathbf{b}_{fg}^T & \mathbf{b}_{fa}^T \end{bmatrix}^T \tag{28}$$

Leader states are assumed to be known without any time lag. The truth and estimate equation pairs are as follows:

$$\dot{\mathbf{q}}_{f|l} = \frac{1}{2}\Xi(\mathbf{q}_{f|l})\boldsymbol{\omega}_{f|l}^f \tag{29a}$$

$$\dot{\hat{\mathbf{q}}}_{f|l} = \frac{1}{2}\Xi(\hat{\mathbf{q}}_{f|l})\hat{\boldsymbol{\omega}}_{f|l}^f \tag{29b}$$

$$\begin{aligned}\ddot{\mathbf{r}}_{f|l}^f = &-[(\dot{\boldsymbol{\omega}}_{f|E}^f)\times]\mathbf{r}_{f|l}^f - [(\boldsymbol{\omega}_{f|I}^f)\times][(\boldsymbol{\omega}_{f|I}^f)\times]\mathbf{r}_{f|l}^f + [(\boldsymbol{\omega}_{f|I}^f \times A_l^f A_E^l \boldsymbol{\omega}_{E|I}^E)\times]\mathbf{r}_{f|l}^f - 2[(\boldsymbol{\omega}_{f|I}^f)\times]\dot{\mathbf{r}}_{f|l}^f \\ &+ \mathbf{a}_f^f - A_l^f \mathbf{a}_l^l + A_l^f A_E^l \left(\mathbf{g}_f^E - \mathbf{g}_l^E\right)\end{aligned} \tag{30a}$$

$$\begin{aligned}\ddot{\hat{\mathbf{r}}}_{f|l}^f = &-[(\dot{\hat{\boldsymbol{\omega}}}_{f|E}^f)\times]\hat{\mathbf{r}}_{f|l}^f - [(\hat{\boldsymbol{\omega}}_{f|I}^f)\times][(\hat{\boldsymbol{\omega}}_{f|I}^f)\times]\hat{\mathbf{r}}_{f|l}^f + [(\hat{\boldsymbol{\omega}}_{f|I}^f \times \hat{A}_l^f A_E^l \boldsymbol{\omega}_{E|I}^E)\times]\hat{\mathbf{r}}_{f|l}^f - 2[(\hat{\boldsymbol{\omega}}_{f|I}^f)\times]\dot{\hat{\mathbf{r}}}_{f|l}^f \\ &+ \hat{\mathbf{a}}_f^f - \hat{A}_l^f \mathbf{a}_l^l + \hat{A}_l^f A_E^l \left(\hat{\mathbf{g}}_f^E - \mathbf{g}_l^E\right)\end{aligned} \tag{30b}$$

$$\mathbf{a}_f^f = \tilde{\mathbf{a}}_f^f - \mathbf{b}_{fa} - \boldsymbol{\eta}_{fav} \tag{31a}$$

$$\hat{\mathbf{a}}_f^f = \tilde{\mathbf{a}}_f^f - \hat{\mathbf{b}}_{fa} \tag{31b}$$

$$\mathbf{g}_f^E = \frac{-\mu}{\|\mathbf{r}_{f|E}^E\|^3}\mathbf{r}_{f|E}^E \tag{32a}$$

$$\hat{\mathbf{g}}_f^E = \frac{-\mu}{\|\hat{\mathbf{r}}_{f|E}^E\|^3}\hat{\mathbf{r}}_{f|E}^E \tag{32b}$$

$$\boldsymbol{\omega}_{f|E}^f = \tilde{\boldsymbol{\omega}}_{f|I}^f - \mathbf{b}_{fg} - \boldsymbol{\eta}_{fgv} - A_l^f A_E^l \boldsymbol{\omega}_{E|I}^E \tag{33a}$$

$$\hat{\boldsymbol{\omega}}_{f|E}^f = \tilde{\boldsymbol{\omega}}_{f|I}^f - \hat{\mathbf{b}}_{fg} - \hat{A}_l^f A_E^l \boldsymbol{\omega}_{E|I}^E \tag{33b}$$

$$\dot{\mathbf{b}}_{fa} = \boldsymbol{\eta}_{fau} \tag{34a}$$

$$\dot{\hat{\mathbf{b}}}_{fa} = \mathbf{0} \tag{34b}$$

$$\dot{\mathbf{b}}_{fg} = \boldsymbol{\eta}_{fgu} \tag{35a}$$

$$\dot{\hat{\mathbf{b}}}_{fg} = \mathbf{0} \tag{35b}$$

The state-error vector is given as

$$\Delta\mathbf{x} \quad = \quad \begin{bmatrix} \boldsymbol{\delta\alpha}_{f|l}^T & (\Delta\mathbf{r}_{f|l}^f)^T & (\Delta\dot{\mathbf{r}}_{f|l}^f)^T & \Delta\mathbf{b}_{fg}^T & \Delta\mathbf{b}_{fa}^T \end{bmatrix}^T \tag{36}$$

The first term is defined by

$$\boldsymbol{\delta\alpha}_{f|l} = 2\boldsymbol{\delta}\mathbf{q}_{f|l_{13}} \tag{37a}$$

$$\boldsymbol{\delta}\mathbf{q}_{f|l} = \mathbf{q}_{f|l} \otimes \hat{\mathbf{q}}_{f|l}^{-1} \tag{37b}$$

where the subscript "$_{13}$" denotes the first three components of the four component vector. This is used due to the assumption that the estimate is close to the truth. For this case, the fourth error-component is approximately one and its derivative is near zero.[22] The remaining state-error terms are defined by

$$\Delta \mathbf{x} = \mathbf{x} - \hat{\mathbf{x}} \tag{38}$$

The process noise vector consists of the four Gaussian noise terms from the measurement equations.

$$\mathbf{w} = \begin{bmatrix} \boldsymbol{\eta}_{fgv}^T & \boldsymbol{\eta}_{fgu}^T & \boldsymbol{\eta}_{fav}^T & \boldsymbol{\eta}_{fau}^T \end{bmatrix}^T \tag{39}$$

The next step is to determine time derivatives of the error states. The equation for $\boldsymbol{\delta}\dot{\boldsymbol{\alpha}}_{f|l}$ is given in Ref. 24 as

$$\boldsymbol{\delta}\dot{\boldsymbol{\alpha}}_{f|l} = -[(\hat{\boldsymbol{\omega}}_{f|l}^f)\times]\boldsymbol{\delta\alpha}_{f|l} + \boldsymbol{\delta\omega}_{f|l}^f \tag{40}$$

where

$$\boldsymbol{\delta\omega}_{f|l}^f = \boldsymbol{\omega}_{f|l}^f - \hat{\boldsymbol{\omega}}_{f|l}^f \tag{41}$$

Based upon the definitions in Eqs. (17) and (33a), along with the approximation

$$A_l^f = (I_{3\times 3} - [(\boldsymbol{\delta\alpha}_{f|l})\times])\hat{A}_l^f \tag{42}$$

Equation (41) becomes

$$\boldsymbol{\delta\omega}_{f|l}^f = -\Delta \mathbf{b}_{fg} - \boldsymbol{\eta}_{fgv} - [(\hat{A}_l^f A_E^l \boldsymbol{\omega}_{E|I}^E + \hat{A}_l^f \boldsymbol{\omega}_{l|E}^l)\times]\boldsymbol{\delta\alpha}_{f|l} \tag{43}$$

Equation (40) then simplifies to

$$\boldsymbol{\delta}\dot{\boldsymbol{\alpha}}_{f|l} = -[(\hat{\boldsymbol{\omega}}_{f|E}^f)\times]\boldsymbol{\delta\alpha}_{f|l} - \Delta \mathbf{b}_{fg} - \boldsymbol{\eta}_{fgv} \tag{44}$$

Time derivative of the position error state vector is simply equal to the velocity error state vector:

$$\frac{d}{dt}(\Delta \mathbf{r}_{f|l}^f) = \Delta \dot{\mathbf{r}}_{f|l}^f \tag{45}$$

The time derivative of the velocity vector is more complicated. To keep this document concise, the algebraic derivation of this equation will be omitted. The final result makes use of several of the relations already mentioned in this paper, along with Euler's equation[20]

$$\dot{\boldsymbol{\omega}}_{f|E}^f = -J_f^{-1}[(\boldsymbol{\omega}_{f|E}^f)\times]J_f \boldsymbol{\omega}_{f|E}^f + J_f^{-1}\mathbf{L}_f \tag{46}$$

where J_f is the inertia matrix of the follower and $\mathbf{L}_f$ is the applied torque. An expansion of the gravity model in Eq. (24) is also required:

$$\mathbf{g}_f^E = \hat{\mathbf{g}}_f^E + \frac{\partial \mathbf{g}_f^E}{\partial \Delta \mathbf{r}_{f|l}^f}\Delta \mathbf{r}_{f|l}^f + \frac{\partial \mathbf{g}_f^E}{\partial \boldsymbol{\delta\alpha}_{f|l}}\boldsymbol{\delta\alpha}_{f|l} \tag{47}$$

where

$$\begin{aligned} \frac{\partial \mathbf{g}_f^E}{\partial \Delta \mathbf{r}_{f|l}^f} &= -\mu A_l^E \hat{A}_f^l \|\mathbf{r}_{l|I}^E + A_l^E \hat{A}_f^l \hat{\mathbf{r}}_{f|l}^f\|^{-3} \\ &\quad -\mu \left(\mathbf{r}_{l|I}^E + A_l^E \hat{A}_f^l \hat{\mathbf{r}}_{f|l}^f\right)\left(-\frac{3}{2}\right)\|\mathbf{r}_{l|I}^E + A_l^E \hat{A}_f^l \hat{\mathbf{r}}_{f|l}^f\|^{-5}\left(2(\mathbf{r}_{l|I}^E)^T A_l^E \hat{A}_f^l + 2(\hat{\mathbf{r}}_{f|l}^f)^T\right) \\ &= -\mu A_l^E \hat{A}_f^l \|\mathbf{r}_{l|I}^E + A_l^E \hat{A}_f^l \hat{\mathbf{r}}_{f|l}^f\|^{-3} \\ &\quad +3\mu \left(\mathbf{r}_{l|I}^E + A_l^E \hat{A}_f^l \hat{\mathbf{r}}_{f|l}^f\right)\left((\mathbf{r}_{l|I}^E)^T A_l^E \hat{A}_f^l + (\hat{\mathbf{r}}_{f|l}^f)^T\right)\|\mathbf{r}_{l|I}^E + A_l^E \hat{A}_f^l \hat{\mathbf{r}}_{f|l}^f\|^{-5} \end{aligned} \tag{48}$$

$$
\begin{aligned}
\frac{\partial \mathbf{g}_f^E}{\partial \boldsymbol{\delta\alpha}_{f|l}} &= -\mu A_l^E[(\hat{A}_f^l\hat{\mathbf{r}}_{f|l}^f)\times]\|\mathbf{r}_{l|I}^E + A_l^E\hat{A}_f^l\hat{\mathbf{r}}_{f|l}^f\|^{-3} - \mu\left(\mathbf{r}_{l|I}^E + A_l^E\hat{A}_f^l\hat{\mathbf{r}}_{f|l}^f\right) \\
&\quad\times\left(-\frac{3}{2}\right)\|\mathbf{r}_{l|I}^E + A_l^E\hat{A}_f^l\hat{\mathbf{r}}_{f|l}^f\|^{-5}\left(2(\mathbf{r}_{l|I}^E)^T A_l^E[(\hat{A}_f^l\hat{\mathbf{r}}_{f|l}^f)\times] + 2(\hat{\mathbf{r}}_{f|l}^f)^T\hat{A}_l^f[(\hat{A}_f^l\hat{\mathbf{r}}_{f|l}^f)\times]\right) \\
&= -\mu A_l^E[(\hat{A}_f^l\hat{\mathbf{r}}_{f|l}^f)\times]\|\mathbf{r}_{l|I}^E + A_l^E\hat{A}_f^l\hat{\mathbf{r}}_{f|l}^f\|^{-3} + 3\mu\left(\mathbf{r}_{l|I}^E + A_l^E\hat{A}_f^l\hat{\mathbf{r}}_{f|l}^f\right) \\
&\quad\times\left((\mathbf{r}_{l|I}^E)^T A_l^E[(\hat{A}_f^l\hat{\mathbf{r}}_{f|l}^f)\times] + (\hat{\mathbf{r}}_{f|l}^f)^T\hat{A}_l^f[(\hat{A}_f^l\hat{\mathbf{r}}_{f|l}^f)\times]\right)\|\mathbf{r}_{l|I}^E + A_l^E\hat{A}_f^l\hat{\mathbf{r}}_{f|l}^f\|^{-5}
\end{aligned}
\tag{49}
$$

Using the above relations, the velocity error dynamics equation is written as

$$
\frac{d}{dt}\Delta\dot{\mathbf{r}}_{f|l}^f = F_{3-1}\boldsymbol{\delta\alpha}_{f|l} + F_{3-2}\Delta\mathbf{r}_{f|l}^f + F_{3-3}\Delta\dot{\mathbf{r}}_{f|l}^f + F_{3-4}\Delta\mathbf{b}_{fg} + F_{3-5}\Delta\mathbf{b}_{fa} + G_{3-1}\boldsymbol{\eta}_{fgv} + G_{3-3}\boldsymbol{\eta}_{fav}
\tag{50}
$$

where

$$
\begin{aligned}
F_{3-1} = &-[(\hat{\mathbf{r}}_{f|l}^f)\times]J_f^{-1}\left\{[(J_f\hat{\boldsymbol{\omega}}_{f|E}^f)\times] - [(\hat{\boldsymbol{\omega}}_{f|E}^f)\times]J_f\right\}[(\hat{A}_l^f A_E^l\boldsymbol{\omega}_{E|I}^E)\times] \\
&- [(\hat{\mathbf{r}}_{f|l}^f)\times][(\tilde{\boldsymbol{\omega}}_{f|I}^f - \hat{\mathbf{b}}_{fg})\times][(\hat{A}_l^f\hat{A}_E^l\boldsymbol{\omega}_{E|I}^E)\times] - [(\hat{A}_l^f\mathbf{a}_l^l)\times] + [(\hat{A}_l^f A_E^l\left(\hat{\mathbf{g}}_f^E - \mathbf{g}_l^E\right))\times] \\
&- \mu\hat{A}_l^f A_E^l\left\{A_l^E[(\hat{A}_f^l\hat{\mathbf{r}}_{f|l}^f)\times]\|\mathbf{r}_{l|I}^E + A_l^E\hat{A}_f^l\hat{\mathbf{r}}_{f|l}^f\|^{-3} - 3\left(\mathbf{r}_{l|I}^E + A_l^E\hat{A}_f^l\hat{\mathbf{r}}_{f|l}^f\right)\right. \\
&\left.\times\left((\mathbf{r}_{l|I}^E)^T A_l^E[(\hat{A}_f^l\hat{\mathbf{r}}_{f|l}^f)\times] + (\hat{\mathbf{r}}_{f|l}^f)^T\hat{A}_l^f[(\hat{A}_f^l\hat{\mathbf{r}}_{f|l}^f)\times]\right)\|\mathbf{r}_{l|I}^E + A_l^E\hat{A}_f^l\hat{\mathbf{r}}_{f|l}^f\|^{-5}\right\}
\end{aligned}
\tag{51a}
$$

$$
\begin{aligned}
F_{3-2} = &-[(\tilde{\boldsymbol{\omega}}_{f|I}^f - \hat{\mathbf{b}}_{fg})\times][(\tilde{\boldsymbol{\omega}}_{f|I}^f - \hat{\mathbf{b}}_{fg})\times] + [((\tilde{\boldsymbol{\omega}}_{f|I}^f - \hat{\mathbf{b}}_{fg})\times\hat{A}_l^f A_E^l\boldsymbol{\omega}_{E|I}^E)\times] - [(\dot{\hat{\boldsymbol{\omega}}}_{f|E}^f)\times] \\
&- \mu\hat{A}_l^f A_E^l\left\{A_l^E\hat{A}_f^l\|\mathbf{r}_{l|I}^E + A_l^E\hat{A}_f^l\hat{\mathbf{r}}_{f|l}^f\|^{-3}\right. \\
&\left.- 3\left(\mathbf{r}_{l|I}^E + A_l^E\hat{A}_f^l\hat{\mathbf{r}}_{f|l}^f\right)\left((\mathbf{r}_{l|I}^E)^T A_l^E\hat{A}_f^l + (\hat{\mathbf{r}}_{f|l}^f)^T\right)\|\mathbf{r}_{l|I}^E + A_l^E\hat{A}_f^l\hat{\mathbf{r}}_{f|l}^f\|^{-5}\right\}
\end{aligned}
\tag{51b}
$$

$$
F_{3-3} = -2[(\tilde{\boldsymbol{\omega}}_{f|I}^f - \hat{\mathbf{b}}_{fg})\times]
\tag{51c}
$$

$$
\begin{aligned}
F_{3-4} = &-[(\hat{\mathbf{r}}_{f|l}^f)\times]J_f^{-1}\left\{[(J_f\hat{\boldsymbol{\omega}}_{f|E}^f)\times] - [(\hat{\boldsymbol{\omega}}_{f|E}^f)\times]J_f\right\} - [(\hat{\mathbf{r}}_{f|l}^f)\times][(\hat{A}_l^f A_E^l\boldsymbol{\omega}_{E|I}^E)\times] - 2[(\dot{\hat{\mathbf{r}}}_{f|l}^f)\times] \\
&- \left([((\tilde{\boldsymbol{\omega}}_{f|I}^f - \hat{\mathbf{b}}_{fg})\times\hat{\mathbf{r}}_{f|l}^f)\times] + [(\tilde{\boldsymbol{\omega}}_{f|I}^f - \hat{\mathbf{b}}_{fg})\times][(\hat{\mathbf{r}}_{f|l}^f)\times]\right)
\end{aligned}
\tag{51d}
$$

$$
F_{3-5} = -I_3
\tag{51e}
$$

$$
\begin{aligned}
G_{3-1} = &-[(\hat{\mathbf{r}}_{f|l}^f)\times]J_f^{-1}\left\{[(J_f\hat{\boldsymbol{\omega}}_{f|E}^f)\times] - [(\hat{\boldsymbol{\omega}}_{f|E}^f)\times]J_f\right\} - [(\hat{\mathbf{r}}_{f|l}^f)\times][(\hat{A}_l^f A_E^l\boldsymbol{\omega}_{E|I}^E)\times] - 2[(\dot{\hat{\mathbf{r}}}_{f|l}^f)\times] \\
&- \left([((\tilde{\boldsymbol{\omega}}_{f|I}^f - \hat{\mathbf{b}}_{fg})\times\hat{\mathbf{r}}_{f|l}^f)\times] + [(\tilde{\boldsymbol{\omega}}_{f|I}^f - \hat{\mathbf{b}}_{fg})\times][(\hat{\mathbf{r}}_{f|l}^f)\times]\right)
\end{aligned}
\tag{51f}
$$

$$
G_{3-3} = -I_3
\tag{51g}
$$

Lastly, the time derivatives of the bias states are found by using Eqs. (34a) through (35b) along with Eq. (38):

$$
\Delta\dot{\mathbf{b}}_{fa} = -\boldsymbol{\eta}_{fau}
\tag{52a}
$$

$$
\Delta\dot{\mathbf{b}}_{fg} = -\boldsymbol{\eta}_{fgu}
\tag{52b}
$$

The overall error dynamics are governed by the equation

$$
\Delta\dot{\mathbf{x}} = F\Delta\mathbf{x} + G\mathbf{w}
\tag{53}
$$

where the F and G matrices are given by

$$F = \begin{bmatrix} -[(\hat{\boldsymbol{\omega}}^f_{f|E})\times] & 0_{3\times3} & 0_{3\times3} & -I_{3\times3} & 0_{3\times3} \\ 0_{3\times3} & 0_{3\times3} & I_{3\times3} & 0_{3\times3} & 0_{3\times3} \\ F_{3-1} & F_{3-2} & F_{3-3} & F_{3-4} & F_{3-5} \\ 0_{3\times3} & 0_{3\times3} & 0_{3\times3} & 0_{3\times3} & 0_{3\times3} \\ 0_{3\times3} & 0_{3\times3} & 0_{3\times3} & 0_{3\times3} & 0_{3\times3} \end{bmatrix} \tag{54a}$$

$$G = \begin{bmatrix} -I_{3\times3} & 0_{3\times3} & 0_{3\times3} & 0_{3\times3} \\ 0_{3\times3} & 0_{3\times3} & 0_{3\times3} & 0_{3\times3} \\ G_{3-1} & 0_{3\times3} & G_{3-3} & 0_{3\times3} \\ 0_{3\times3} & I_{3\times3} & 0_{3\times3} & 0_{3\times3} \\ 0_{3\times3} & 0_{3\times3} & 0_{3\times3} & I_{3\times3} \end{bmatrix} \tag{54b}$$

The covariance matrix used in the EKF is

$$Q = \begin{bmatrix} \sigma^2_{fgv} I_{3\times3} & 0_{3\times3} & 0_{3\times3} & 0_{3\times3} \\ 0_{3\times3} & \sigma^2_{fguv} I_{3\times3} & 0_{3\times3} & 0_{3\times3} \\ 0_{3\times3} & 0_{3\times3} & \sigma^2_{fav} I_{3\times3} & 0_{3\times3} \\ 0_{3\times3} & 0_{3\times3} & 0_{3\times3} & \sigma^2_{fau} I_{3\times3} \end{bmatrix} \tag{55}$$

A discrete propagation is used for the covariance matrix in order to reduce the computational load:

$$P^-_{k+1} = \Phi_k P^+_k \Phi^T_k + \mathcal{Q}_k \tag{56}$$

where Φ_k is the state transition matrix and $\mathcal{Q}_k$ is the covariance matrix. Van Loan (See Ref. 25) gives a numerical solution for these matrices. The first step is to set up the following $2n$ by $2n$ matrix:

$$\mathcal{A} = \begin{bmatrix} -F & GQG^T \\ 0_{n\times n} & F^T \end{bmatrix} \Delta t \tag{57}$$

The matrix exponential is then calculated:

$$\mathcal{B} = e^{\mathcal{A}} = \begin{bmatrix} \mathcal{B}_{11} & \mathcal{B}_{12} \\ 0_{n\times n} & \mathcal{B}_{22} \end{bmatrix} = \begin{bmatrix} \mathcal{B}_{11} & \Phi^{-1}_k \mathcal{Q}_k \\ 0_{n\times n} & \Phi^T_k \end{bmatrix} \tag{58}$$

The state transition and covariance matrices are then given as

$$\Phi_k = \mathcal{B}^T_{22} \tag{59a}$$
$$\mathcal{Q}_k = \Phi_k \mathcal{B}_{12} \tag{59b}$$

VI. Measurement Equations

The measurements used in this filter consist of the relative LOS observations between the two UAVs. A schematic of this system is shown in Fig. 2. Beacons are located on the follower at coordinates specified in the follower reference frame by (X_i, Y_i, Z_i).

The relation between image space measurements of the PSD to the object space are given by[26]

$$\alpha_i = -f \frac{A_{11}(X_i + x) + A_{12}(Y_i + y) + A_{13}(Z_i + z)}{A_{31}(X_i + x) + A_{32}(Y_i + y) + A_{33}(Z_i + z)} \tag{60a}$$
$$\beta_i = -f \frac{A_{21}(X_i + x) + A_{22}(Y_i + y) + A_{23}(Z_i + z)}{A_{31}(X_i + x) + A_{32}(Y_i + y) + A_{33}(Z_i + z)} \tag{60b}$$

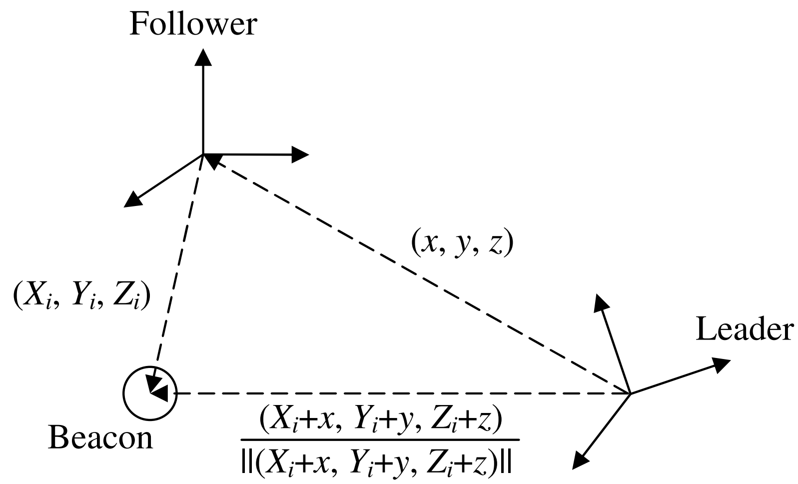

Figure 2. Vision Based Navigation System

where f is the focal length, and the A matrix transforms from the follower frame to the leader frame and is therefore equal to $(A_l^f)^T$. Writing these equations in terms of A_l^f yields

$$\alpha_i = -f \frac{A^f_{l_{11}}(X_i + x) + A^f_{l_{21}}(Y_i + y) + A^f_{l_{31}}(Z_i + z)}{A^f_{l_{13}}(X_i + x) + A^f_{l_{23}}(Y_i + y) + A^f_{l_{33}}(Z_i + z)} \tag{61a}$$

$$\beta_i = -f \frac{A^f_{l_{12}}(X_i + x) + A^f_{l_{22}}(Y_i + y) + A^f_{l_{32}}(Z_i + z)}{A^f_{l_{13}}(X_i + x) + A^f_{l_{23}}(Y_i + y) + A^f_{l_{33}}(Z_i + z)} \tag{61b}$$

Since observations can be given as α_i/f and β_i/f, the focal length is set equal to one in order to simplify the math. The (x, y, z) coordinates are the components of the vector $\mathbf{r}^f_{f|l}$.

Consider a measurement vector denoted by

$$\tilde{\boldsymbol{\gamma}}_i = \boldsymbol{\gamma}_i + \mathbf{v} \tag{62a}$$

$$\boldsymbol{\gamma}_i \equiv \begin{bmatrix} \alpha_i \\ \beta_i \end{bmatrix} \tag{62b}$$

A frequently used covariance of $\mathbf{v}$ is given by Ref. 27 as

$$R_i^{\text{FOCAL}} = \frac{\sigma^2}{1 + d(\alpha_i^2 + \beta_i^2)} \begin{bmatrix} (1 + d\alpha_i^2)^2 & (d\alpha_i\beta_i)^2 \\ (d\alpha_i\beta_i)^2 & (1 + d\beta_i^2)^2 \end{bmatrix} \tag{63}$$

where d is on the order of 1 and σ is assumed to be known. Note that the components of this covariance matrix will increase as the image space coordinates increase. This demonstrates that errors will increase as the observation moves away from the boresight. Reference 27 also states that for practical purposes, the estimated values of α_i and β_i must be used in place of the true quantities. This only leads to second order error effects.

The problem with using Eq. (62a) as the measurement vector is that the definitions of α_i and β_i in Eqs. (61a) and (61b) are highly nonlinear in both the position and attitude components. A simpler observation vector is given in unit vector form as

$$\mathbf{b}_i = (A_l^f)^T \mathbf{r}_i \tag{64}$$

where

$$\mathbf{r}_i \equiv \frac{1}{\sqrt{(X_i + x)^2 + (Y_i + y)^2 + (Z_i + z)^2}} \begin{bmatrix} X_i + x \\ Y_i + y \\ Z_i + z \end{bmatrix} \tag{65}$$

and for a sensor facing in the positive Z direction,

$$\mathbf{b}_i = \frac{1}{\sqrt{1+\alpha_i^2+\beta_i^2}} \begin{bmatrix} -\alpha_i \\ -\beta_i \\ 1 \end{bmatrix} \tag{66}$$

Similar equations for the positive X and Y directions are found by rotating the elements of the vector in a cyclic manner. Sensors facing in the negative direction use the same equations multiplied by negative one.

In Ref. 28, Shuster and Oh showed that when measurement noise is present, nearly all the probability errors are concentrated on a small area about the direction of $\mathbf{b}_i$, allowing the sphere containing that point to be approximated by a tangent plane. The measurement vector is defined as

$$\tilde{\mathbf{b}}_i = \mathbf{b}_i + \boldsymbol{\nu}_i \tag{67}$$

where the sensor error $\boldsymbol{\nu}_i$ is assumed Gaussian with

$$E\{\boldsymbol{\nu}_i\} = 0 \tag{68a}$$

$$R_i^{\text{QUEST}} \equiv E\{\boldsymbol{\nu}_i \boldsymbol{\nu}_i^T\} = \sigma^2 (I_{3\times 3} - \mathbf{b}_i \mathbf{b}_i^T) \tag{68b}$$

Equation (68b) is known as the QUEST measurement model. Once again, this is a function of the true values since $\mathbf{b}_i$ is present. The matrix R_i^{QUEST} is also a singular matrix, which causes singularity issues in the gain computation of the EKF. In Ref. 29, Shuster showed that the measurement covariance can effectively be replaced by $\sigma^2 I_{3\times 3}$, which is both non-singular and not a function of true state values.

The QUEST measurement model works well for small field of view sensors, but may produce significant errors for larger field of views, such as the VISNAV sensor. A new covariance model is developed in Ref. 30 that provides better accuracy than the QUEST model for this case. It is based upon a first-order Taylor series expansion of the unit vector observation. The primary assumption is that the measurement noise is small compared to the signal. The new covariance is defined as

$$R_i^{\text{NEW}} = J_i R_i^{\text{FOCAL}} J_i^T \tag{69}$$

where J_i is the Jacobian of Eq. (66) and is given by

$$J_i \equiv \frac{\partial \mathbf{b}_i}{\partial \boldsymbol{\gamma}_i} = \frac{1}{\sqrt{1+\alpha_i^2+\beta_i^2}} \begin{bmatrix} -1 & 0 \\ 0 & -1 \\ 0 & 0 \end{bmatrix} - \frac{1}{1+\alpha_i^2+\beta_i^2} \mathbf{b}_i \begin{bmatrix} \alpha_i & \beta_i \end{bmatrix} \tag{70}$$

Appropriate modifications to the Jacobian must be made for sensors facing along the other axes. It should be noted that R_i^{NEW} is also a singular matrix. This issue must be overcome before the covariance can be used within the EKF framework. A rank-one update approach is shown effective to overcome this difficulty, as shown in Ref. 30. The basic idea is to add an additional term $c_i \mathbf{b}_i \mathbf{b}_i^T$ ($c_i > 0$) to the measurement covariance matrix to ensure that the new covariance matrix is nonsingular and does not change the overall result in the EKF. This is mathematically written as

$$\mathcal{R}_i^{\text{NEW}} = R_i^{\text{NEW}} + c_i \mathbf{b}_i \mathbf{b}_i^T \tag{71}$$

The coefficient c_i is recommended to be given by

$$c_i = \frac{1}{2} \text{trace}(R_i^{\text{NEW}}) \tag{72}$$

where trace is the mathematical function denoting trace of a matrix.

The next step is to determine the partial of the measurement vector with respect to the state vector in order to form the H matrix of the filter. Using Eq. (42), Eq. (64) becomes

$$\begin{aligned} \mathbf{b}_i &= (\hat{A}_l^f)^T (I_{3\times 3} + [(\boldsymbol{\delta\alpha}_{f|l})\times])\mathbf{r}_i \\ &= (\hat{A}_l^f)^T \mathbf{r}_i + (\hat{A}_l^f)^T [(\boldsymbol{\delta\alpha}_{f|l})\times]\mathbf{r}_i \\ &= (\hat{A}_l^f)^T \mathbf{r}_i - (\hat{A}_l^f)^T [(\mathbf{r}_i)\times]\boldsymbol{\delta\alpha}_{f|l} \end{aligned} \tag{73}$$

Table 1. Summary of Extended Kalman Filter for Relative Inertial Navigation

Initialize	$\hat{\mathbf{q}}_{fl}(t_0) = \mathbf{q}_{f\|l0}$ $\hat{\mathbf{r}}^f_{f\|l}(t_0) = \mathbf{r}^f_{f\|l0}$ $\hat{\mathbf{v}}^f_{f\|l}(t_0) = \mathbf{v}^f_{f\|l0}$ $\boldsymbol{\beta}_{fg}(t_0) = \boldsymbol{\beta}_{fg0}$ $\boldsymbol{\beta}_{fa}(t_0) = \boldsymbol{\beta}_{fa0}$ $P(t_0) = P_0$
Gain	$K_k = P_k^- H_k^T(\hat{\mathbf{x}}_k^-)[H_k(\hat{\mathbf{x}}_k^-)P_k^- H_k^T(\hat{\mathbf{x}}_k^-) + R_k]^{-1}$ $H_k(\hat{\mathbf{x}}_k^-) = \left[\begin{array}{ccccc} \frac{\partial \mathbf{b}_i}{\partial \boldsymbol{\delta\alpha}_l^f} & \frac{\partial \mathbf{b}_i}{\partial \mathbf{r}^f_{f\|l}} & 0_{3\times3} & 0_{3\times3} & 0_{3\times3} \end{array} \right] \Big\|_{t_k}$
Update	$P_k^+ = [I - K_k H_k(\hat{\mathbf{x}}^-)]P_k^-$ $\Delta\hat{\tilde{\mathbf{x}}}_k^+ = K_k[\tilde{\mathbf{y}}_k - \hat{\mathbf{y}}_k^-]$ $\Delta\hat{\tilde{\mathbf{x}}}_k^+ \equiv \left[\begin{array}{ccccc} \boldsymbol{\delta\alpha}^{+T}_{f\|l_k} & \Delta\mathbf{r}^f_{f\|l_k} & \Delta\mathbf{v}^f_{f\|l_k} & \Delta\boldsymbol{\beta}^{+T}_{fg_k} & \Delta\boldsymbol{\beta}^{+T}_{fa_k} \end{array} \right]$ $\hat{\mathbf{q}}^+_{f\|l_k} = \hat{\mathbf{q}}^-_{f\|l_k} + \frac{1}{2}\Xi(\hat{\mathbf{q}}^-_{f\|l_k})\boldsymbol{\delta\alpha}_{f\|l_k}$ $\hat{\mathbf{q}}^+_{f\|l_k} = \frac{\hat{\mathbf{q}}^+_{f\|l_k}}{\\|\hat{\mathbf{q}}^+_{f\|l_k}\\|}$ $\hat{\mathbf{r}}^{f+}_{f\|l_k} = \hat{\mathbf{r}}^{f-}_{f\|l_k} + \Delta\mathbf{r}^f_{f\|l_k}$ $\hat{\mathbf{v}}^{f+}_{f\|l_k} = \hat{\mathbf{v}}^{f-}_{f\|l_k} + \Delta\mathbf{v}^f_{f\|l_k}$ $\hat{\boldsymbol{\beta}}^+_{fg_k} = \hat{\boldsymbol{\beta}}^-_{fg_k} + \Delta\hat{\boldsymbol{\beta}}^+_{fg_k}$ $\hat{\boldsymbol{\beta}}^+_{fa_k} = \hat{\boldsymbol{\beta}}^-_{fa_k} + \Delta\hat{\boldsymbol{\beta}}^+_{fa_k}$
Propagation	$\hat{\mathbf{a}}^{f+}_{f_k} = \tilde{\mathbf{a}}^f_{f_k} - \hat{\boldsymbol{\beta}}^+_{fa_k}$ $\hat{\boldsymbol{\omega}}^{f+}_{f\|l_k} = \tilde{\boldsymbol{\omega}}^f_{f\|I_k} - \hat{A}^f_l \boldsymbol{\omega}^l_{l\|E_k} - \hat{\boldsymbol{\beta}}^+_{fg_k}$ $\hat{\mathbf{q}}^-_{f\|l_{k+1}} = \bar{\Omega}(\hat{\boldsymbol{\omega}}^+_{f\|l_k})\bar{\Gamma}(\hat{\boldsymbol{\omega}}^+_{f\|l_k})\hat{\mathbf{q}}^+_{f\|l_k}$ $P^-_{k+1} = \Phi_k P_k^+ \Phi_k^T + \mathcal{Q}_k$ $\ddot{\hat{\mathbf{r}}}^f_{f\|l} = -[(\dot{\hat{\boldsymbol{\omega}}}^f_{f\|E})\times]\hat{\mathbf{r}}^f_{f\|l} - [(\hat{\boldsymbol{\omega}}^f_{f\|I})\times][(\hat{\boldsymbol{\omega}}^f_{f\|I})\times]\hat{\mathbf{r}}^f_{f\|l} + [(\hat{\boldsymbol{\omega}}^f_{f\|I} \times \hat{A}^f_l A^l_E \boldsymbol{\omega}^E_{E\|I})\times]\hat{\mathbf{r}}^f_{f\|l}$ $-2[(\hat{\boldsymbol{\omega}}^f_{f\|I})\times]\dot{\hat{\mathbf{r}}}^f_{f\|l} + \hat{\mathbf{a}}^f_f - \hat{A}^f_l \mathbf{a}^l_l + \hat{A}^f_l A^l_E \left(\hat{\mathbf{g}}^E_f - \mathbf{g}^E_l\right)$ $\hat{\mathbf{g}}^E_f = \frac{-\mu}{\\|\hat{\mathbf{r}}^E_{f\|E}\\|^3}\hat{\mathbf{r}}^E_{f\|E}$

The partial derivative with respect to the attitude states is simply given by

$$\frac{\partial \mathbf{b}_i}{\partial \boldsymbol{\delta\alpha}_l^f} = -(\hat{A}^f_l)^T[(\mathbf{r}_i)\times] \tag{74}$$

The partial derivative with respect to the position vector is more complicated, and given by Ref. 18:

$$\begin{aligned} \frac{\partial \mathbf{b}_i}{\partial \mathbf{r}^f_{f|l}} &= (A^f_l)^T \frac{\partial \mathbf{r}_i}{\partial \mathbf{r}^f_{f|l}} \\ &= (A^f_l)^T \frac{1}{C} L \end{aligned} \tag{75}$$

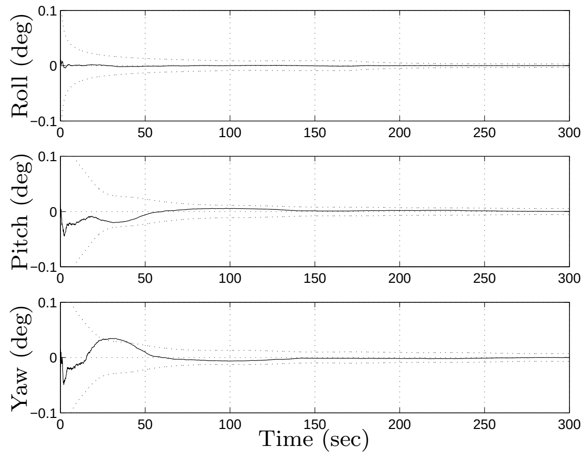

(a) Angle Errors (3 Beacons)

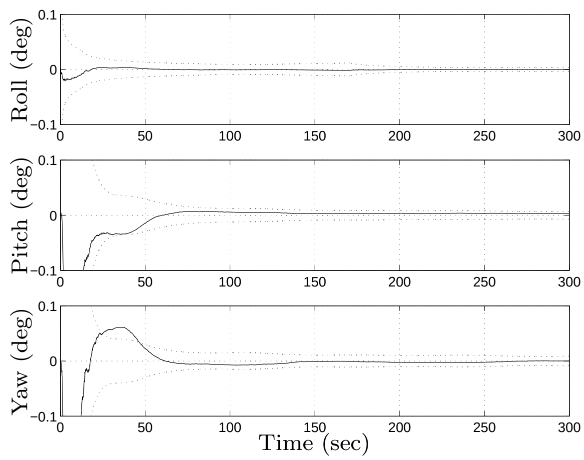

(b) Angle Errors (2 Beacons)

Figure 3. Relative Attitude Errors (Scenario I)

where C and the elements of the matrix L are given by

$$C = \left[(X_i + x)^2 + (Y_i + y)^2 + (Z_i + z)^2\right]^{3/2} \tag{76a}$$

$$L_{11} = [(Y_i + y)^2 + (Z_i + z)^2] \tag{76b}$$

$$L_{12} = L_{21} = -(X_i + x)(Y_i + y) \tag{76c}$$

$$L_{13} = L_{31} = -(X_i + x)(Z_i + z) \tag{76d}$$

$$L_{22} = [(X_i + x)^2 + (Z_i + z)^2] \tag{76e}$$

$$L_{23} = L_{32} = -(Y_i + y)(Z_i + z) \tag{76f}$$

$$L_{33} = [(X_i + x)^2 + (Y_i + y)^2] \tag{76g}$$

The overall H matrix is then given as

$$H_i = \begin{bmatrix} \dfrac{\partial \mathbf{b}_i}{\partial \boldsymbol{\delta\alpha}_l^f} & \dfrac{\partial \mathbf{b}_i}{\partial \mathbf{r}_{f|l}^f} & 0_{3\times 3} & 0_{3\times 3} & 0_{3\times 3} \end{bmatrix} \tag{77}$$

The complete extended Kalman filter is summarized in Table 1, where R_k is the block-diagonal matrix made up of all the individual $\mathcal{R}_{i_k}^{\text{NEW}}$ matrices, and $\tilde{\mathbf{y}}_k \equiv [\tilde{\mathbf{b}}_{1_k}^T \ \cdots \ \tilde{\mathbf{b}}_{N_k}^T]^T$ and $\hat{\mathbf{y}}_k^- \equiv [\hat{\mathbf{b}}_{1_k}^{-T} \ \cdots \ \hat{\mathbf{b}}_{N_k}^{-T}]^T$, where N is the total number of LOS observations at time t_k.

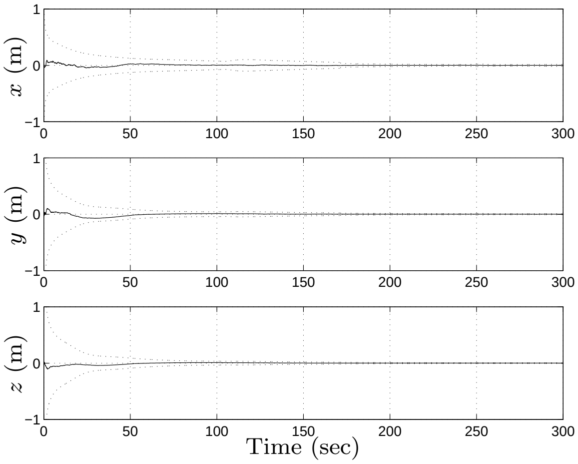

(a) Relative Position Errors (3 Beacons)

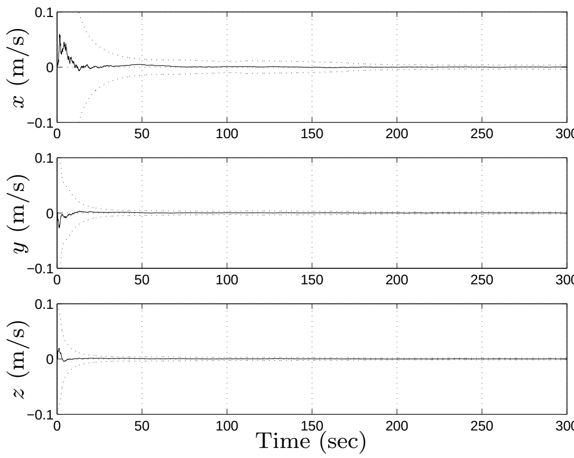

(b) Relative Velocity Errors (3 Beacons)

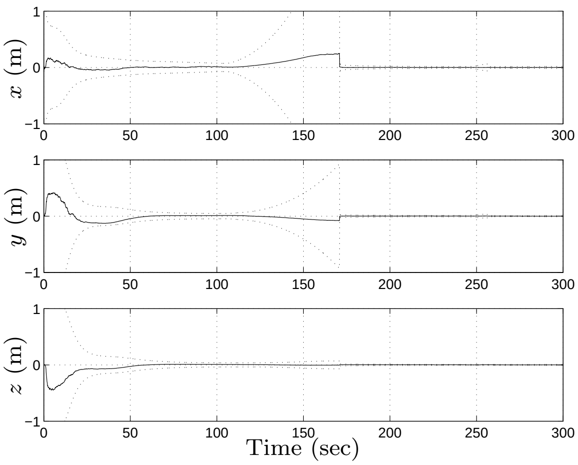

(c) Relative Position Errors (2 Beacons)

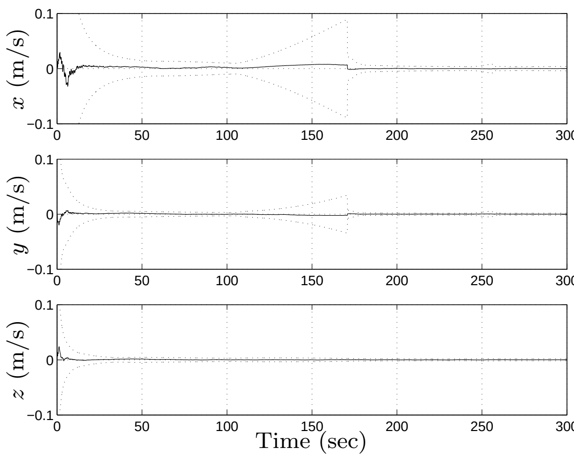

(d) Relative Velocity Errors (2 Beacons)

Figure 4. Kinematic Errors (Scenario I)

VII. Modified Kalman Filter

A modification to the previously derived extended Kalman filter will also be tested. Since the relative distance between the leader and follower is small compared to the radius of the Earth, there is a possibility that the gravity terms will be negligible. To remove the gravity terms from the filter, Eqs. (51a) through (51g) are reexamined. It can be seen that only the F_{3-1} and F_{3-2} terms need to be modified. Their new values are given by

$$\begin{aligned} F_{3-1} = &-[(\hat{\mathbf{r}}^f_{f|l})\times]J_f^{-1}\left\{[(J_f\hat{\boldsymbol{\omega}}^f_{f|E})\times] - [(\hat{\boldsymbol{\omega}}^f_{f|E})\times]J_f\right\}[(\hat{A}^f_l A^l_E \boldsymbol{\omega}^E_{E|I})\times] \\ &- [(\hat{\mathbf{r}}^f_{f|l})\times][(\tilde{\boldsymbol{\omega}}^f_{f|I} - \hat{\mathbf{b}}_{fg})\times][(\hat{A}^f_l A^l_E \boldsymbol{\omega}^E_{E|I})\times] - [(\hat{A}^f_l \mathbf{a}^l_l)\times] \end{aligned} \tag{78a}$$

$$F_{3-2} = -[(\tilde{\boldsymbol{\omega}}^f_{f|I} - \hat{\mathbf{b}}_{fg})\times][(\tilde{\boldsymbol{\omega}}^f_{f|I} - \hat{\mathbf{b}}_{fg})\times] + [((\tilde{\boldsymbol{\omega}}^f_{f|I} - \hat{\mathbf{b}}_{fg}) \times \hat{A}^f_l A^l_E \boldsymbol{\omega}^E_{E|I})\times] - [(\dot{\hat{\boldsymbol{\omega}}}^f_{f|E})\times] \tag{78b}$$

The remainder of the filter is the same and is given by Table 1.

VIII. Simulations

This section shows simulation results for a leader/follower pair of UAVs. Trajectories are defined in the NED reference frame for a location of interest at $\lambda = 38$ degrees and $\phi = -77$ degrees over a five minute

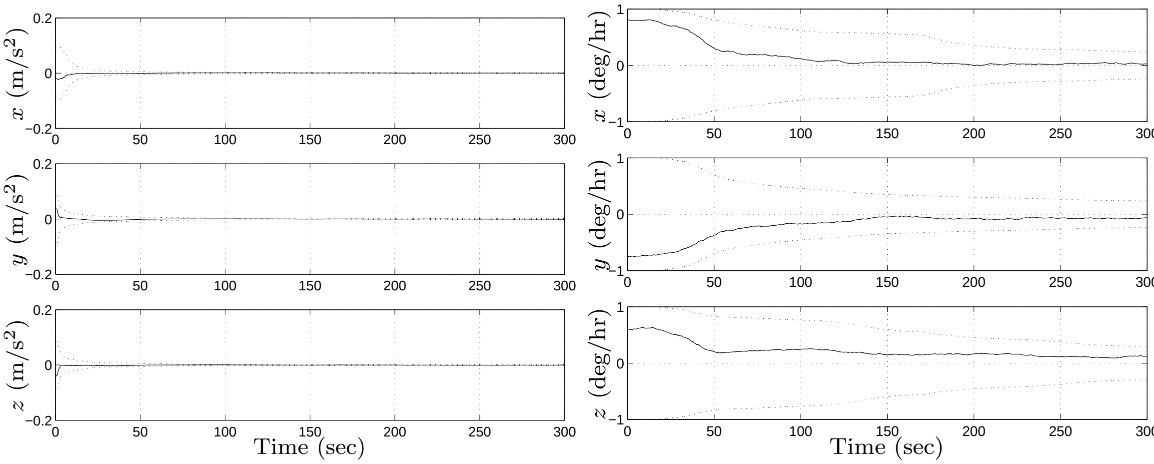

(a) Accelerometer Bias Errors (3 Beacons) (b) Gyro Bias Errors (3 Beacons)

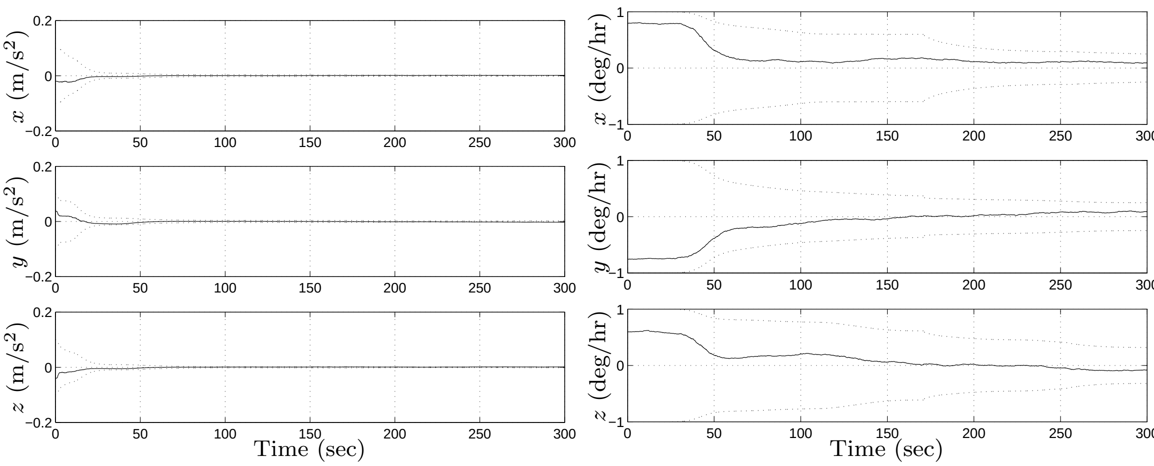

(c) Accelerometer Bias Errors (2 Beacons) (d) Gyro Bias Errors (2 Beacons)

Figure 5. Bias Errors (Scenario I)

period. The position trajectories are given by

$$\mathbf{r}_{l|N}^{N} = \begin{bmatrix} 50t + 5\cos(0.01t) \\ 1000\sin(0.05t) \\ -10t \end{bmatrix} \tag{79a}$$

$$\mathbf{r}_{f|l}^{N} = \begin{bmatrix} 50t + 5\cos(0.01t) + 30\cos(0.1t + \frac{\pi}{6}) + 100) \\ 1000\sin(0.05t) + 20\cos(0.1t) + 100 \\ -10t + 40\cos(0.1t + \frac{\pi}{4}) \end{bmatrix} \tag{79b}$$

They are then converted to the ECEF frame using Eq. (4). The leader and follower UAVs are given the following constant rotational rates:

$$\boldsymbol{\omega}_{l|I}^{l} = \begin{bmatrix} 1 & 1 & 1 \end{bmatrix}^T \ \frac{\text{deg}}{\text{min}} \tag{80a}$$

$$\boldsymbol{\omega}_{f|I}^{f} = \begin{bmatrix} -10 & 5 & -2.5 \end{bmatrix}^T \ \frac{\text{deg}}{\text{min}} \tag{80b}$$

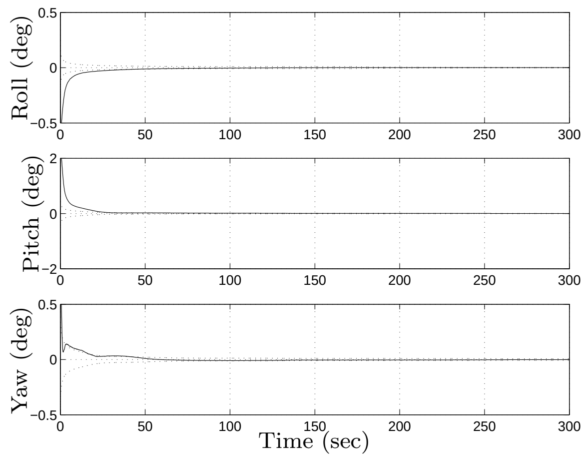

(a) Angle Errors (3 Beacons)

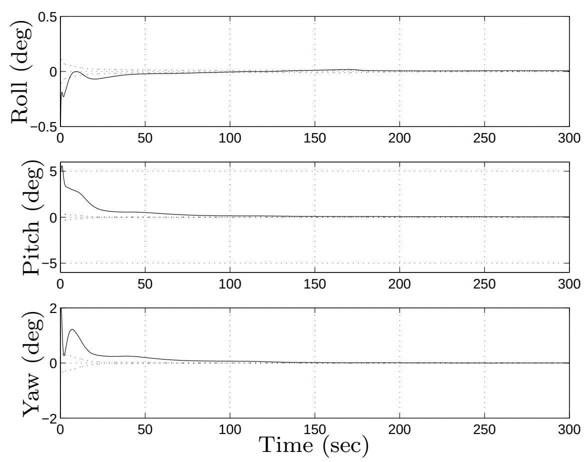

(b) Angle Errors (2 Beacons)

Figure 6. Relative Attitude Errors (Scenario II)

The initial quaternion attitude parameters are given as

$$\mathbf{q}_{l|E} = \begin{bmatrix} -\frac{1}{2} & \frac{1}{2\sqrt{2}} & -\frac{1}{2\sqrt{2}} & \frac{\sqrt{2}}{2} \end{bmatrix}^T \tag{81a}$$

$$\mathbf{q}_{f|E} = \begin{bmatrix} \frac{1}{2\sqrt{3}} & \frac{1}{2\sqrt{3}} & \frac{1}{2\sqrt{3}} & \frac{\sqrt{3}}{2} \end{bmatrix}^T \tag{81b}$$

Gyro, accelerometer and relative position measurements are taken every 0.1 seconds. The gyro noise parameters are $\sigma_{gv} = 8.7266 \times 10^{-7} \frac{\text{rad}}{\text{s}^{1/2}}$ and, $\sigma_{gu} = 2.15 \times 10^{-8} \frac{\text{rad}}{\text{s}^{3/2}}$. The accelerometer noise parameters are $\sigma_{av} = 1.5 \times 10^{-5} \frac{\text{m}}{\text{s}^{3/2}}$ and, $\sigma_{au} = 6.0 \times 10^{-5} \frac{\text{m}}{\text{s}^{5/2}}$. The initial gyro and accelerometer biases are given by

$$\boldsymbol{\beta}_{fg} = [\ 0.8 \quad -0.75 \quad 0.6\ ]^T \ \frac{\text{deg}}{\text{s}} \tag{82a}$$

$$\boldsymbol{\beta}_{fa} = [\ -0.002 \quad 0.0375 \quad -0.004\ ]^T \ \frac{\text{m}}{\text{s}^2} \tag{82b}$$

Both the accelerometer and gyro biases are initially assumed to be zero. The initial covariance matrix P_0 is diagonal. The attitude components of the covariance are initialized to a 3σ bound of 1 degree. The position and velocity parts have 3σ bounds of 20 meters and 0.5 meters per second, respectively. The accelerometer and gyro bias components have 3σ bounds 1 degree per hour and 0.1 meters per second squared, respectively. Scenarios will be tested with varying numbers of beacons, with locations given in Table 2.

Scenarios with the following sets of initial condition errors will be tested on the full EKF:

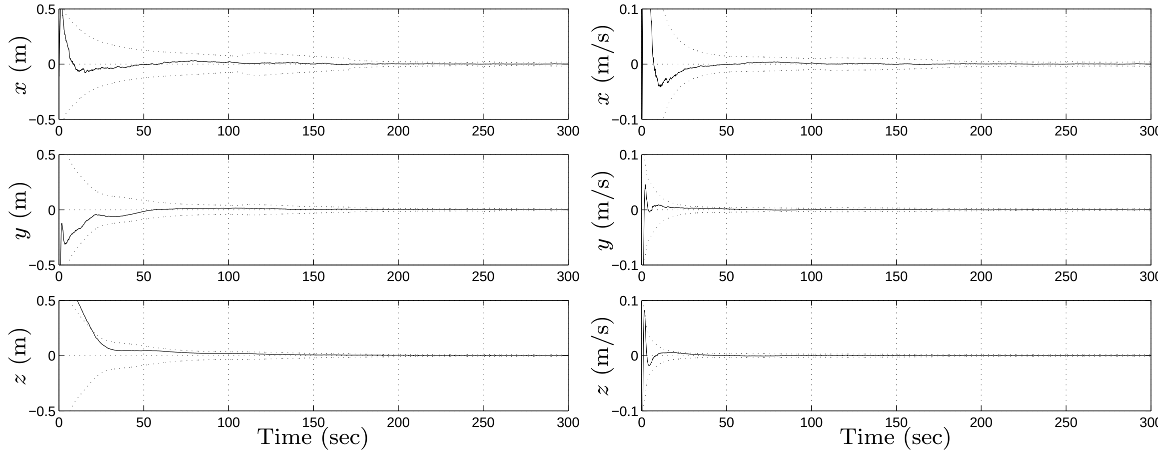

(a) Relative Position Errors (3 Beacons) (b) Relative Velocity Errors (3 Beacons)

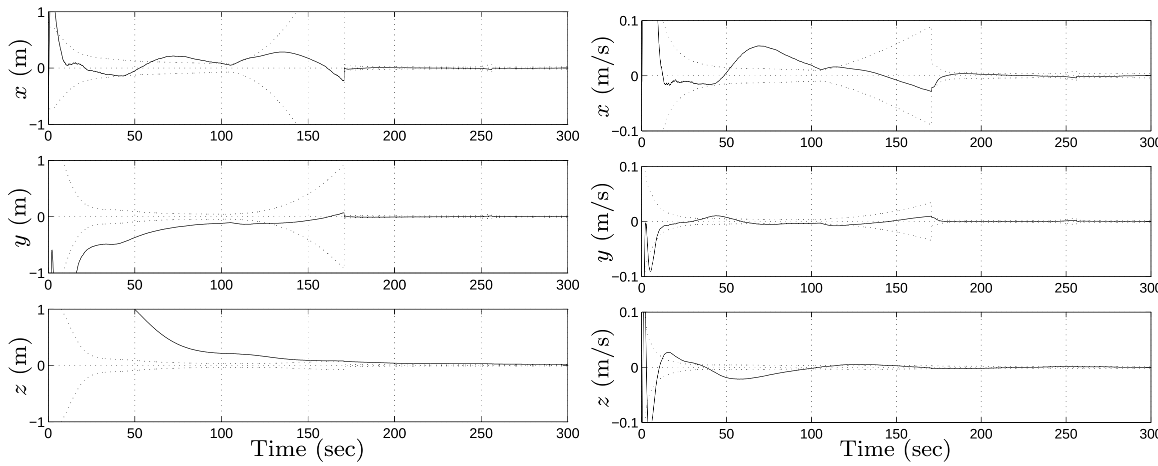

(c) Relative Position Errors (2 Beacons) (d) Relative Velocity Errors (2 Beacons)

Figure 7. Kinematic Errors (Scenario II)

Table 2. List of Beacon Locations

Beacon Number (i)	X_i	Y_i	Z_i
1	0 m	7 m	0 m
2	0 m	-7 m	0 m
3	3.75 m	0 m	0 m
4	-3.75 m	0 m	0 m
5	-3.75 m	-2.25 m	-1.5 m
6	-3.75 m	2.25 m	-1.5 m
7	1.5 m	0 m	0 m
8	-1.5m	0 m	0 m

I Gyro bias and accelerometer bias

II Relative quaternion and both biases

III Relative position, relative velocity and both biases

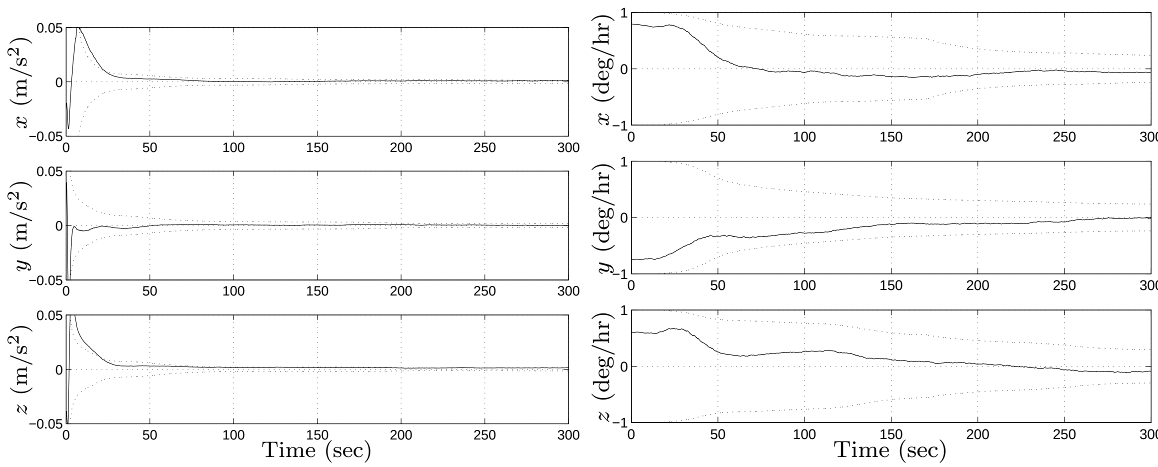

(a) Accelerometer Bias Errors (3 Beacons) (b) Gyro Bias Errors (3 Beacons)

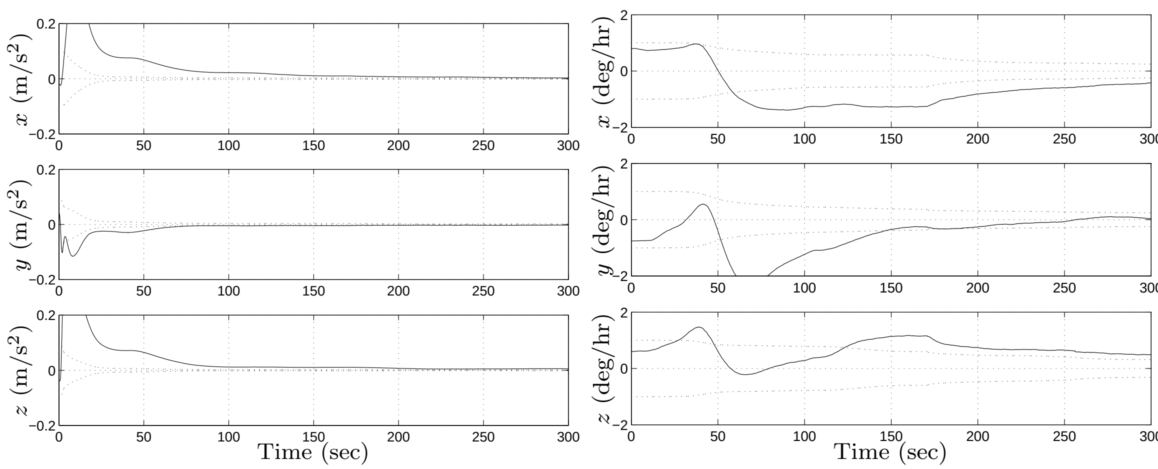

(c) Accelerometer Bias Errors (2 Beacons) (d) Gyro Bias Errors (2 Beacons)

Figure 8. Bias Errors (Scenario II)

IV All states

For all scenarios, plots are shown of the two and three beacon cases. The use of only one beacon is insufficient for estimator convergence, while higher numbers of beacons simply yield lower errors and tighter covariance bounds. Figures 3 through 5 show the results of scenario one where the only initial condition errors present are on the bias terms. The angle errors corresponding to the error quaternion are shown in Fig. 3. All states are seen to converge quickly within their covariance bounds. The primary reason for showing the two beacon case is seen in Fig. 4. The two beacon case is seen to have an intermediate increase in covariance in both the relative position and relative velocity states. Three beacons is needed to maintain smooth covariance bounds.

The second scenario uses an initial quaternion given by

$$\hat{\mathbf{q}}^{f}_{f|l}(t_0) = \boldsymbol{\delta}\mathbf{q} \otimes \mathbf{q}^{f}_{f|l}(t_0) \tag{83}$$

where

$$\boldsymbol{\delta}\mathbf{q} = \begin{bmatrix} \boldsymbol{\delta}\mathbf{a} \\ 1 \end{bmatrix} \tag{84a}$$

$$\boldsymbol{\delta}\mathbf{a} = \begin{bmatrix} 1 & -2 & -2 \end{bmatrix}^T \times \frac{\pi}{180} \tag{84b}$$

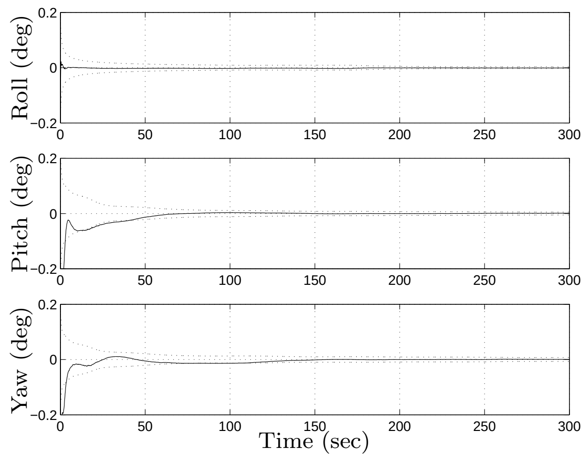

(a) Angle Errors (3 Beacons)

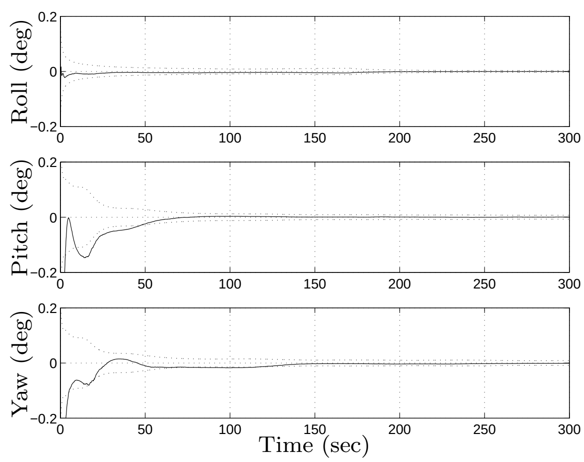

(b) Angle Errors (2 Beacons)

Figure 9. Relative Attitude Errors (Scenario III)

Figures 6 through 8 show the resulting errors for the two and three beacon scenarios. Convergence occurred for all states, though it took significantly longer for the two beacon case. The same intermediate covariance increase can be seen in the two beacon case for the relative position and relative velocity states.

The next scenario contains initial condition errors in the relative position and velocity. These errors are given by

$$\hat{\mathbf{r}}^f_{f|l}(t_0) = 0.9\mathbf{r}^f_{f|l}(t_0) \tag{85}$$

$$\hat{\mathbf{v}}^f_{f|l}(t_0) = \mathbf{v}^f_{f|l}(t_0) + \begin{bmatrix} 5 & -5 & 3 \end{bmatrix}^T \text{ m/s} \tag{86}$$

Results of the two and three beacons cases are shown in Figs. 9 through 11. The relative position and relative velocity errors of Fig. 10 show the same intermediate covariance increase for the two beacon case. The two most significant features of these plots are that the errors are smaller than that of scenario two, and the states remain within their covariance bounds for a much greater percentage of the simulation.

Scenario four simply uses all of the previously stated initial condition errors. The results of the three beacon case are shown in Figs. 12 through 14. The estimate errors and covariance bounds are seen to be similar to that of scenario two. The use of three beacons again allows all states to be estimated effectively and quickly. These figures also demonstrate that initial condition errors in the relative quaternion have more influence that initial condition errors on the relative position and relative velocity.

The final simulations are of the extended Kalman filter that was modified to remove gravity-related terms. As was seen in previous simulations, one beacon was insufficient to achieve accurate estimates while

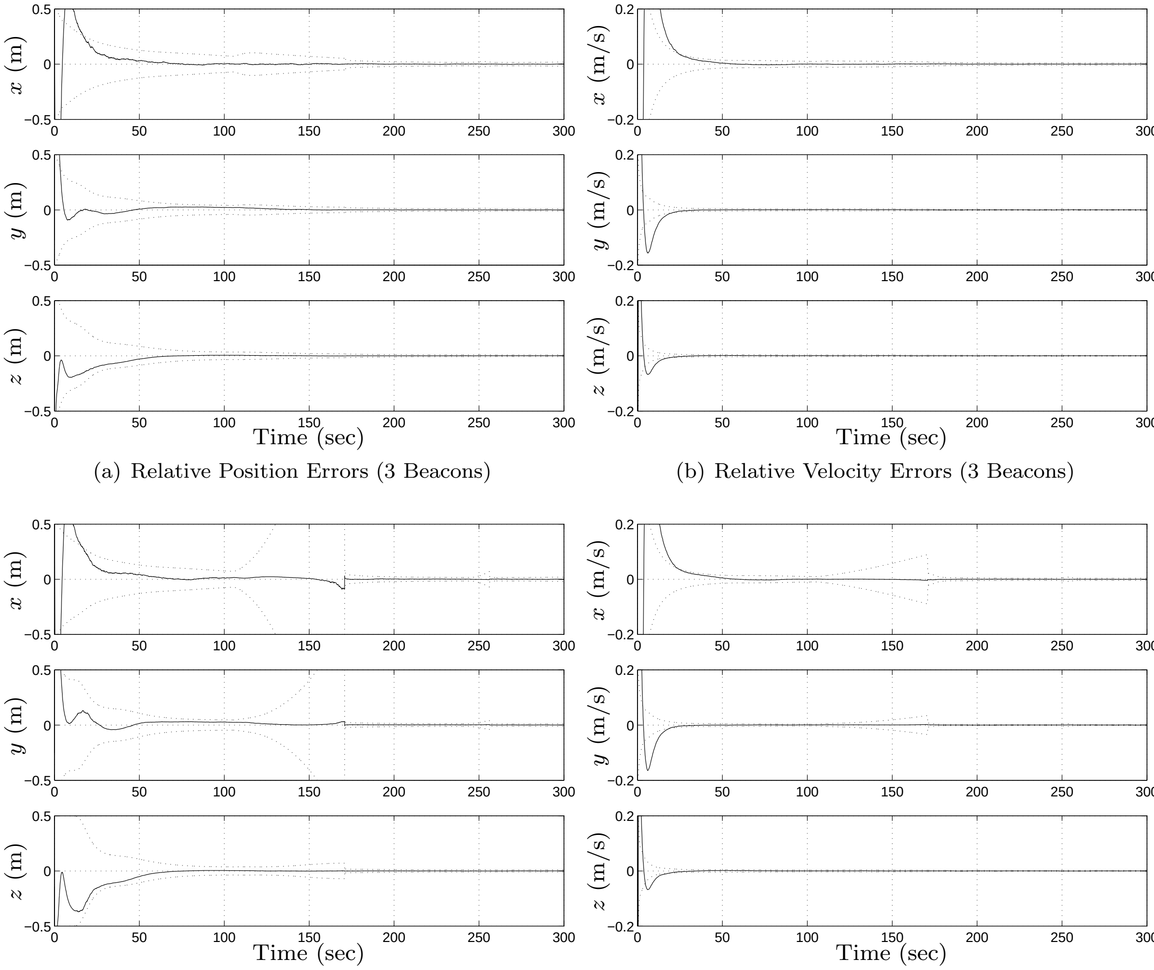

(a) Relative Position Errors (3 Beacons)

(b) Relative Velocity Errors (3 Beacons)

(c) Relative Position Errors (2 Beacons)

(d) Relative Velocity Errors (2 Beacons)

Figure 10. Kinematic Errors (Scenario III)

two beacons resulted in an intermediate covariance increase. The results of the three beacon case are shown in Figs. 15 through 17. Comparing these with the prior simulations, they are seen to be nearly identical to that of Figs. 9 through 11. This shows that the absence of gravity terms has the same effect as initial condition errors in the relative position and relative velocity.

IX. Conclusion

An extended Kalman filter is derived for the relative navigation of uninhabited autonomous vehicles. Relative attitude is parameterized using a quaternion. Its estimation is reduced from four states to three by using a multiplicative error quaternion. Measurements are taken by simulating visual navigation beacons. These beacons are assumed to be placed on the follower while the sensors are on board the leader. Simulations are performed using a number of beacons ranging from one to eight.

For all simulations, estimator convergence occurred only when two or more beacons were present. The use of two beacons showed some states to converge from outside of the covariance bounds, several of which requiring a significant amount of time to actually converge. Adding initial condition errors to the relative position and relative velocity yielded no observable difference. The most notable feature occurred in the relative position and relative velocity states for the two beacon simulations. An intermediate increase in the covariances was observed. This is likely due to a physical arrangement of the beacons with respect to the leader that temporarily made these states unobservable.

The final set of simulations used the extended Kalman filter modified to remove all gravity related terms.

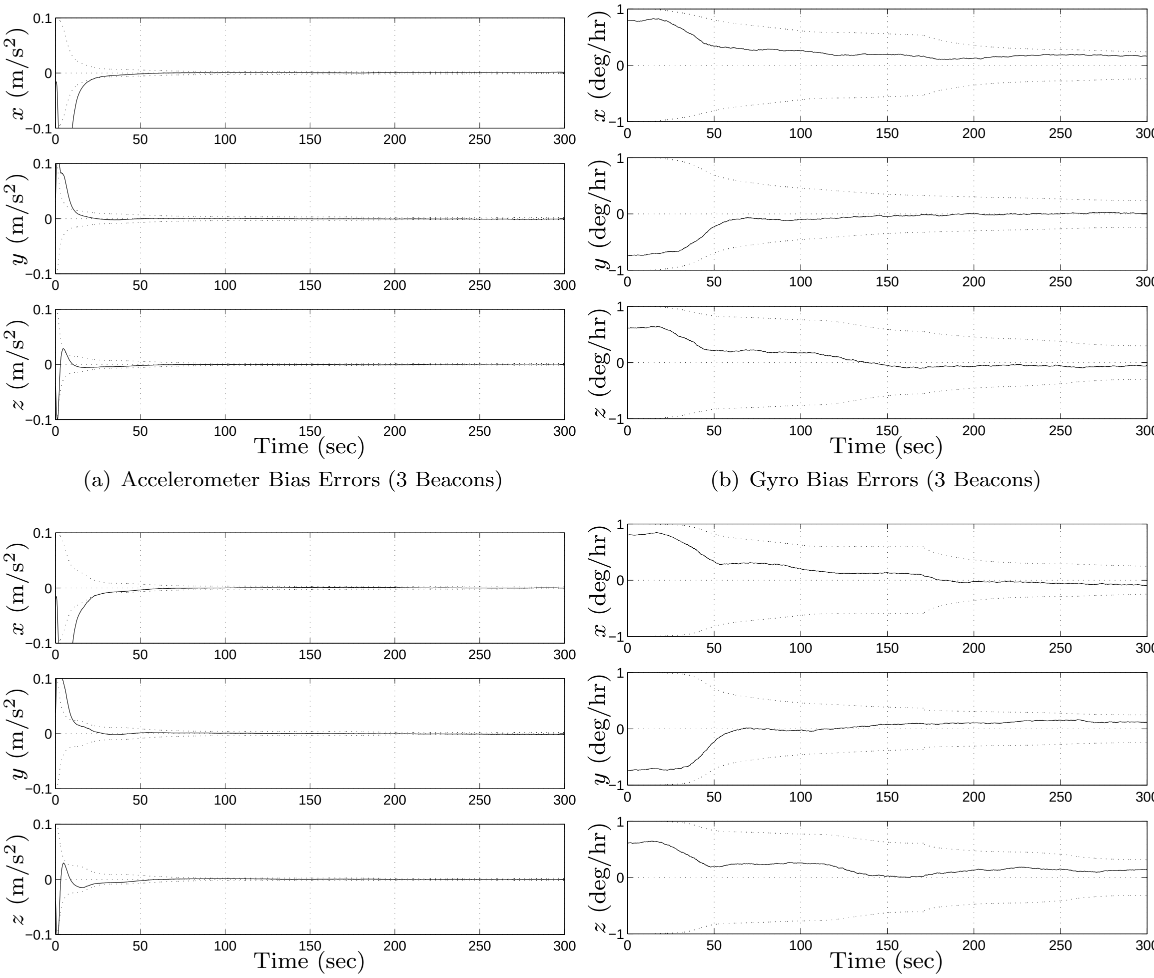

(a) Accelerometer Bias Errors (3 Beacons)

(b) Gyro Bias Errors (3 Beacons)

(c) Accelerometer Bias Errors (2 Beacons)

(d) Gyro Bias Errors (2 Beacons)

Figure 11. Bias Errors (Scenario III)

The only initial condition errors present were on the bias terms. Results showed that this filter is comparable to the full version scenario where initial condition errors in the relative position and relative velocity were added. The use of one beacon was insufficient for producing accurate estimates, while the results of the two beacon case showed the same intermediate covariance increase seen in previous simulations. Overall, the derived filter has been shown effective in a variety of scenarios. The use of three beacons allows accurate estimates to be achieved for any set of testing conditions.

References

[1] Proud, A. W., Pachter, M., and D'Azzo, J. J., "Close Formation Flight Control," *AIAA Guidance, Navigation and Control Conference*, 1999.

[2] Schumacher, C. J. and Kumar, R., "Adaptive Control of UAVs in Close-Coupled Formation Flight," *American Control Conference*, Chicago, IL, June 2000, pp. 849–853.

[3] Singh, S. N., Chandler, P., Schumacher, C., Banda, S., and Pachter, M., "Adaptive Feedback Linearizing Nonlinear Close Formation Control of UAVs," *American Control Conference*, Chicago, IL, Jun. 2000, pp. 854–858.

[4] Boskovic, J. D., Li, S. M., and Mehra, R. K., "Semi-Globally Stable Formation Flight Control Design in Three Dimensions," *40th IEEE Conference on Decision and Control*, Vol. 2, Orlando, FL, Dec. 2001, pp. 1059–1064.

[5] Hall, J. K. and Pachter, M., "Formation Maneuvers in Three Dimensions," *AIAA Guidance, Navigation and Control Conference*, Denver, CO, Aug. 2000, AIAA-2000-4372.

[6] Johnson, E. N., Calise, A. J., Sattigeri, R., Watanabe, Y., and Madyastha, V., "Approaches to Vision-Based Formation Control," *43th IEEE Conference on Decision and Control*, Vol. 2, Paradise Island, Bahamas, Dec. 2004, pp. 1643–1648.

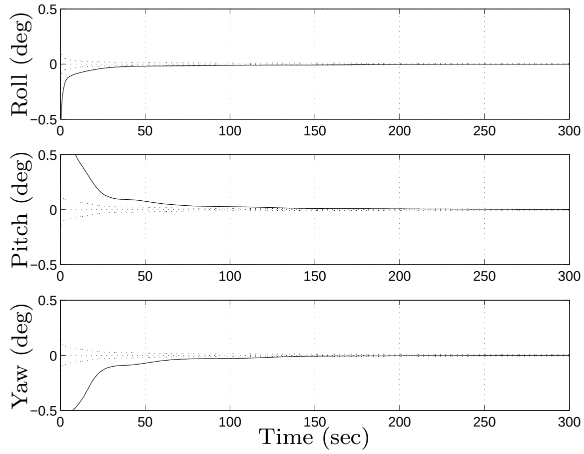

Figure 12. Relative Attitude Errors (Scenario IV)

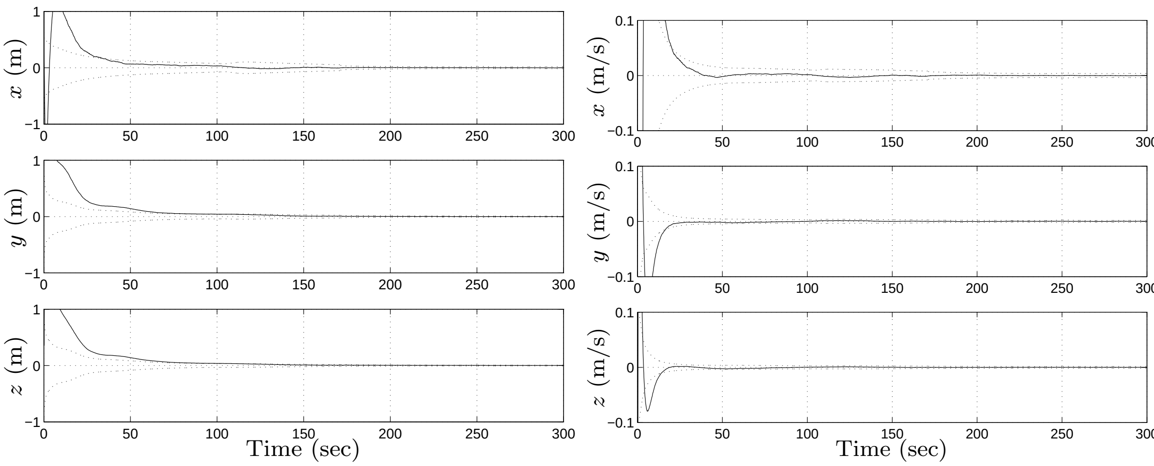

(a) Relative Position Errors (3 Beacons)

(b) Relative Velocity Errors (3 Beacons)

Figure 13. Kinematic Errors (Scenario IV)

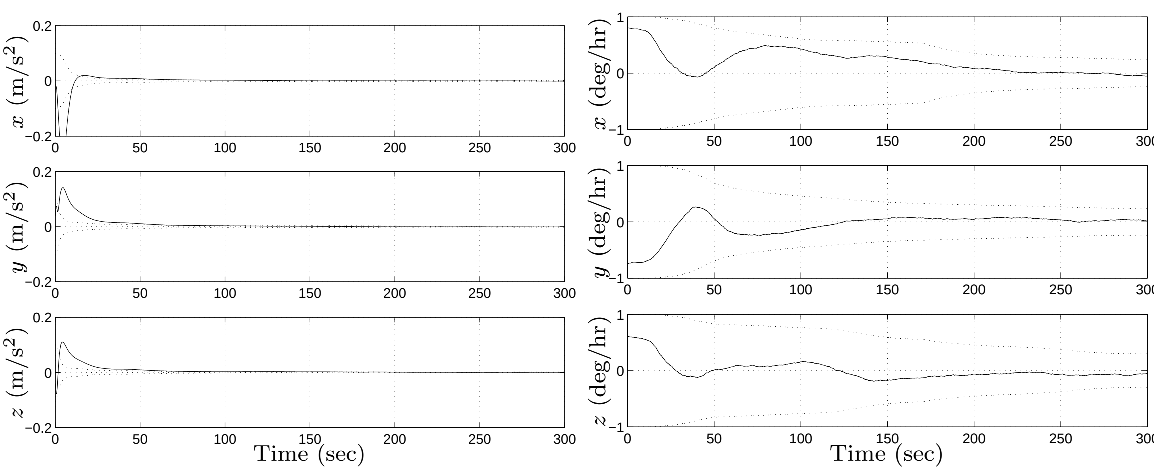

(a) Accelerometer Bias Errors (3 Beacons)

(b) Gyro Bias Errors (3 Beacons)

Figure 14. Bias Errors (Scenario IV)

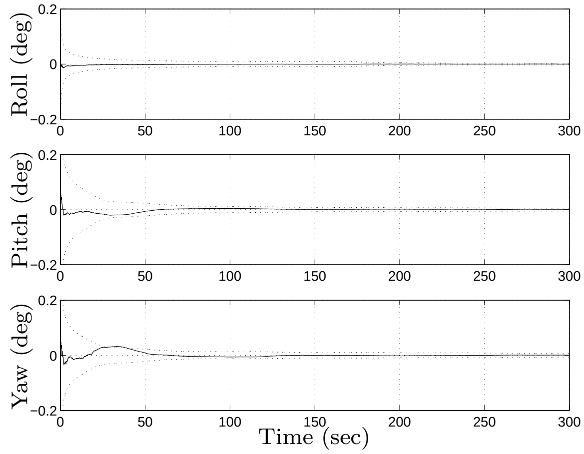

Figure 15. Relative Attitude Errors (Modified EKF)

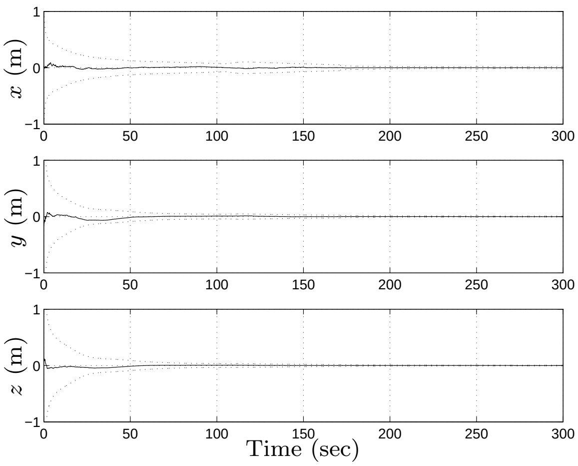

(a) Relative Position Errors (3 Beacons)

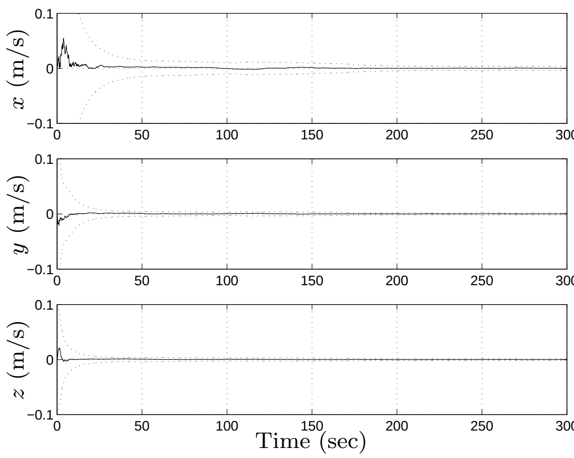

(b) Relative Velocity Errors (3 Beacons)

Figure 16. Kinematic Errors (Modified EKF)

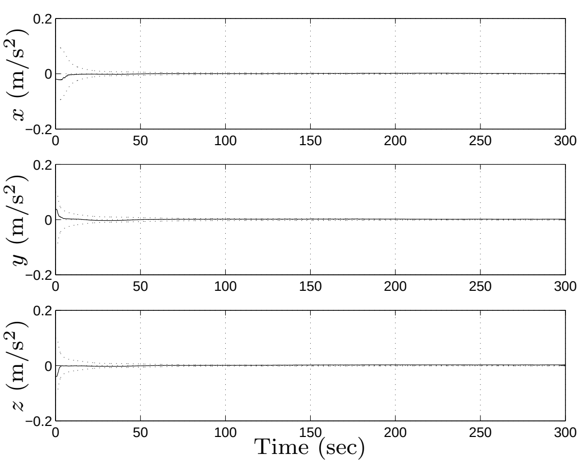

(a) Accelerometer Bias Errors (3 Beacons)

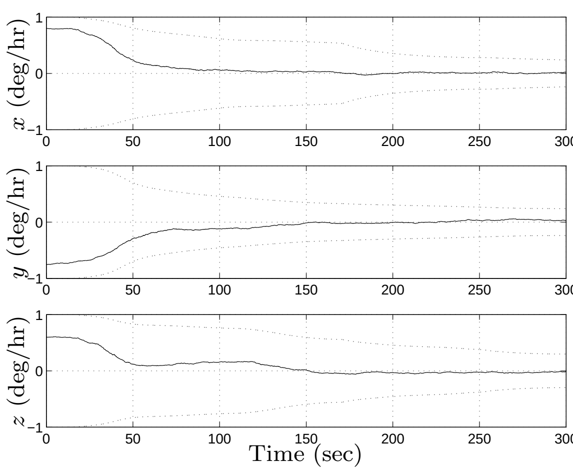

(b) Gyro Bias Errors (3 Beacons)

Figure 17. Bias Errors (modified EKF)

[7]Aidala, V. J. and Hammel, S. E., "Utilization of Modified Polar Coordinates for Bearings-Only Tracking," *IEEE Transactions on Automatic Control*, Vol. 28, No. 3, March 1983, pp. 283–294.

[8]Chatfield, A. B., *Fundamentals of High Accuracy Inertial Navigation*, American Institute of Aeronautics and Astronautics, Inc., Reston, VA, 1997.

[9]Connelly, J., Kourepenis, A., Marinis, T., and Hanson, D., "Micromechanical Sensors in Tactical GN&C Applications," *AIAA Guidance, Navigation and Contol Conference*, Montreal, QB, Canada, Aug. 2001, AIAA-2001-4407.

[10]Farrell, J. and Barth, M., *The Global Positioning System and Inertial Navigation*, McGraw-Hill, New York, NY, 1998.

[11]Crassidis, J. L., "Sigma-Point Kalman Filtering for Integrated GPS and Inertial Navigation," *AIAA Guidance, Navigation, and Control Conference*, San Francisco, CA, Aug. 2005, AIAA-05-6052.

[12]Gustafsson, F., Gunnarsson, F., Bergman, N., Forssell, U., Jansson, J., Karlsson, R., and Nordlund, P.-J., "Particle Filters for Positioning, Navigation, and Tracking," *IEEE Transactions on Signal Processing*, Vol. 50, No. 2, Feb. 2002, pp. 425–435.

[13]Felter, S. C. and Wu, N. E., "A Relative Navigation System for Formation Flight," *IEEE Transactions on Aerospace and Electronic Systems*, Vol. 33, No. 3, July 1997, pp. 958–967.

[14]Woo, M. J. and Choi, J. W., "A Relative Navigation System for Vehicle Plattoning," *40th SICE Annual Conference*, Nagoya, Japan, July 2001, pp. 28–31.

[15]Junkins, J. L., Hughes, D. C., Wazni, K. P., and Pariyapong, V., "Vision-Based Navigation for Rendezvous, Docking and Proximity Operations," *22nd Annual AAS Guidance and Control Conference*, Breckenridge, CO, Feb. 1999, AAS-99-021.

[16]Alonso, R., Crassidis, J. L., and Junkins, J. L., "Vision-Based Relative Navigation for Formation Flying of Spacecraft," *AIAA Guidance, Navigation, and Control Conference*, Denver, CO, Aug. 2000, AIAA-00-4439.

[17]Crassidis, J. L., Alonso, R., and Junkins, J. L., "Optimal Attitude and Position Determination from Line-of-Sight Measurements," *The Richard H. Battin Astrodynamics Conference*, College Station, TX, Mar. 2000, AAS-00-268.

[18]Kim, S. G., Crassidis, J. L., Cheng, Y., and Fosbury, A. M., "Kalman Filtering for Relative Spacecraft Attitude and Position Estimation," *AIAA Guidance, Navigation, and Control Conference*, San Francisco, CA, Aug. 2005, AIAA-2005-6087.

[19]Haas, B. M., *Sensitivity Study: The Effects of Beacon Location Errors on a Vehicle's Position and Attitude Estimation for a Vision-Based Navigation System*, Master's thesis, University at Buffalo, State University of New York, May 2005.

[20]Schaub, H. and Junkins, J. L., *Analytical Mechanics of Aerospace Systems*, American Institute of Aeronautics and Astronautics, Inc., New York, NY, 2003.

[21]Shuster, M. D., "A Survey of Attitude Representations," *Journal of the Astronautical Sciences*, Vol. 41, No. 4, Oct.-Dec. 1993, pp. 439–517.

[22]Lefferts, E. J., Markley, F. L., and Shuster, M. D., "Kalman Filtering for Spacecraft Attitude Estmation," *Journal of Guidance, Control, and Dynamics*, Vol. 5, No. 5, Sept.-Oct. 1982.

[23]Mayo, R. A., "Relative Quaternion State Transition Relation," *Journal of Guidance and Control*, Vol. 2, No. 1, Jan.-Feb. 1979, pp. 44–48.

[24]Fosbury, A. M., *Control of Relative Attitude Dynamics of a Formation Flight Using Model-Error Control Synthesis*, Master's thesis, University at Buffalo, State University of New York, March 2005.

[25]Van-Loan, C. F., "Computing Integrals Involving Matrix Exponentials," *IEEE Transactions on Automatic Control*, Vol. AC-23, No. 3, Jun. 1978, pp. 396–404.

[26]Light, D. L., "Satellite Photogtammetry," *Maunual of Photogrammetry*, edited by C. C. Slama, chap. 17, American Society of Photogrammetry, Falls Church, VA, 4th ed., 1980.

[27]Shuster, M. D., "Kalman Filtering of Spacecraft Attitude and the QUEST Model," *Journal of the Astronautical Sciences*, Vol. 38, No. 3, July-Sept. 1990.

[28]Shuster, M. D. and Oh, S. D., "Three Axis Attitude Determination from Vector Observations," *Journal of Guidance, Navigation and Control*, Vol. 4, No. 1, Jan-Feb. 1981.

[29]Shuster, M. D., "Kalman Filtering of Spacecraft Attitude and the QUEST Model," *Journal of the Astronautical Sciences*, Vol. 38, No. 3, 1990, pp. 377–393.

[30]Cheng, Y., Crassidis, J. L., and Markley, F. L., "Attitude Estimation for Large Field-of-View Sensors," *AAS Malcolm D. Shuster Astronautics Symposium*, Grand Island, NY, June 2005, AAS-2005-462.